12-2011

Analyzing Spring Freeze Impacts on Deciduous Forest Productivity Using MODIS Satellite Imagery

Karl Lintvedt
University of Arkansas, Fayetteville

ANALYZING SPRING FREEZE IMPACTS ON DECIDUOUS FOREST PRODUCTIVITY USING MODIS SATELLITE IMAGERY

ANALYZING SPRING FREEZE IMPACTS ON DECIDUOUS FOREST PRODUCTIVITY USING MODIS SATELLITE IMAGERY

A thesis submitted in partial fulfillment
of the requirements for the degree of
Master of Arts in Geography

By

Karl Anders Lintvedt
San Diego State University
Bachelor of Arts in Geography, 2006

December 2011
University of Arkansas

ABSTRACT

The impacts of an April 2007 spring freeze event on the productivity of deciduous broadleaf forest were analyzed using geographic information system (GIS) tools. Forest productivity was modeled using the Enhanced Vegetation Index (EVI), as recorded by the Moderate Resolution Imaging Spectroradiometer (MODIS) satellite sensor. Measures of spatial autocorrelation were used to quantify the degree of spatial congruence between a map depicting the severity of the freeze event, and maps modeling forest productivity throughout the year. The results show a geographic correlation between the unseasonably low minimum temperatures sustained during the freeze and the unusually low forest productivity that followed. Discussion also includes the influence on freeze damage of premature growth onset triggered by an unusually warm March 2007, the seemingly paradoxical relationship between spring frost damage and climate change, and the potential for practical applications of this study with regard to predictive modeling and ecological forecasting.

Keywords: spring, freeze, frost, deciduous, forest, photosynthesis, raster, spatial autocorrelation, Moran's I, MODIS, EVI, GIS.

This thesis is approved for recommendation
to the Graduate Council.

Thesis Director:

_____

Dr. Jason Tullis

Thesis Committee:

_____

Dr. Jason Tullis

_____

Dr. Jackson Cothren

_____

Dr. Kenneth Kvamme

THESIS DUPLICATION RELEASE

I hereby authorize the University of Arkansas Libraries to duplicate this thesis when needed for research and/or scholarship.

Agreed _____
Karl Lintvedt

Refused _____
Karl Lintvedt

TABLE OF CONTENTS

I. INTRODUCTION

A. The April 2007 Freeze Event

This study is concerned with the biophysical impact of a North American weather event that occurred over Easter weekend, April 2007. The weather pattern produced unseasonably cold freezing temperatures that were low enough and sufficiently long-lived to dramatically reduce vegetative health throughout the central and southern United States. However, for a comprehensive understanding of the factors that contributed to the impacts associated with this record-setting cold wave, an accurate account must begin a month prior, during an abnormally warm March.

Due to a dominant ridge of high atmospheric pressure that stretched from the Northern Plains to the Southeast, March 2007 was, on average, warmer than a typical March by more than 9°F (NOAA, 2007). During the week prior to the freeze in central Missouri, at a time when daily minimum temperature (TMIN) is typically in the low 40s, temperatures did not drop below 59°F. At the Walker Branch weather station in central Tennessee, TMIN exceeded 59°F eight times during the two weeks prior to the freeze, a time when TMIN there is normally 42°F (NOAA, 2007). Tennessee's daily high temperatures for late March were also well above average, ranging between 70-80°F (Windham, 2008). In fact, March 2007 would ultimately prove to be the single warmest March on record at Tennessee's Walker Branch weather station, as well as the nearby Oak Ridge station (Gu, 2008).

The prolonged March warmth caused vegetation to break its winter dormancy and begin its spring "green-up" phase earlier than normal. This led to the premature emergence of agricultural crops, the premature blooming of seasonal plants and flowers, and of particular

interest to this study, the premature flushing of tree leaves among deciduous hardwood forests throughout the region.

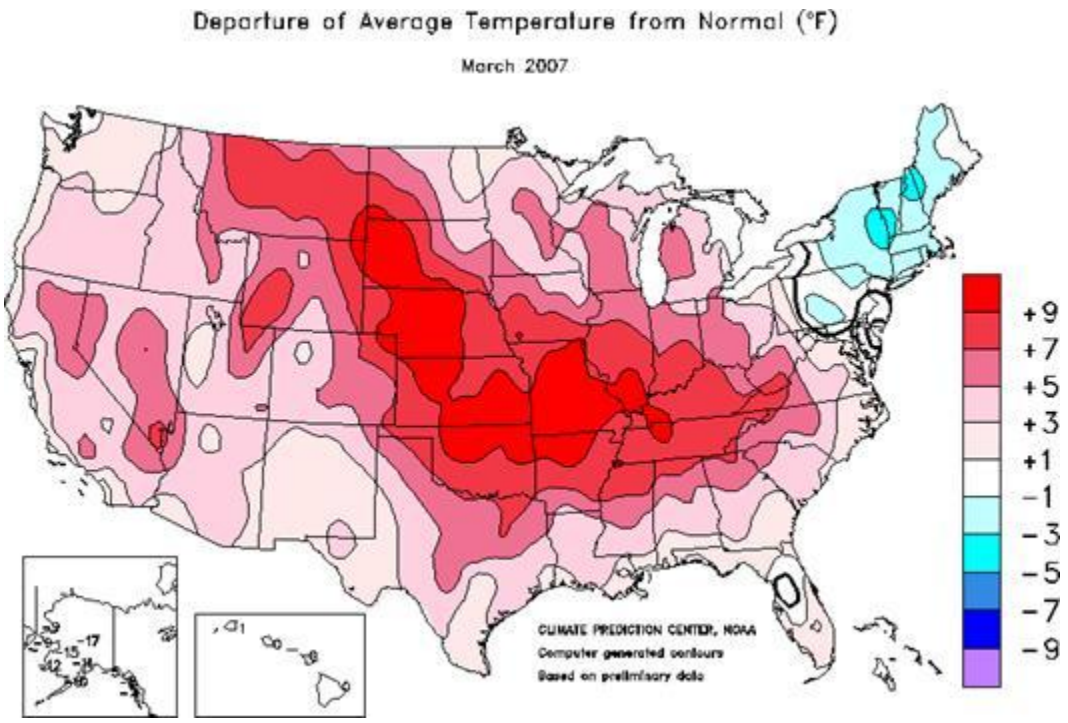

Figure 1-1 Temperature anomaly map depicting the unusually warm March 2007 temperatures (in red) that contributed to premature spring growth onset across the U.S. interior. (NOAA, 2010)

Weather patterns changed dramatically on April 4, 2007. Directly following the period of record-setting, growth-triggering warmth, a slow-moving mass of arctic air moved south from Canada into the interior of the continental United States. The strong upper level jet stream responsible for this cold front remained in place for days, including throughout the Easter weekend. The pattern eventually subsided on April 10, when the upper level jet decayed and the appearance of a low pressure system over the central plains caused air flow to shift from a northerly direction to the west/southwest, effectively ending the freeze.

During the time that had elapsed, the cold surface air that blanketed the region had produced several days' worth of record-setting low temperatures throughout many central plains, midwest, and southeastern states. Temperatures well below freezing were recorded at weather stations across the region, including reports of TMIN into the twenties and teens for some places. Throughout 17 states, as many as 1,237 TMIN records were broken, and 321 were tied (NOAA, 2007). During the period of April 6-9, average daily low temperatures in the South were 24, 20, 16, and 18°F, respectively (University of Tennessee, 2010). In Crossville, Tennessee, temperatures continuously remained at or below freezing for a cumulative total of 70 hours (Windham, 2008). In Fayetteville, Arkansas, record low TMIN of 21 and 17°F were set on April 7th and 8th, respectively – the latter of which was 27 degrees below the daily normal TMIN of 44°F, and to this day remains Fayetteville's all-time record low for the month of April (NOAA, 2007).

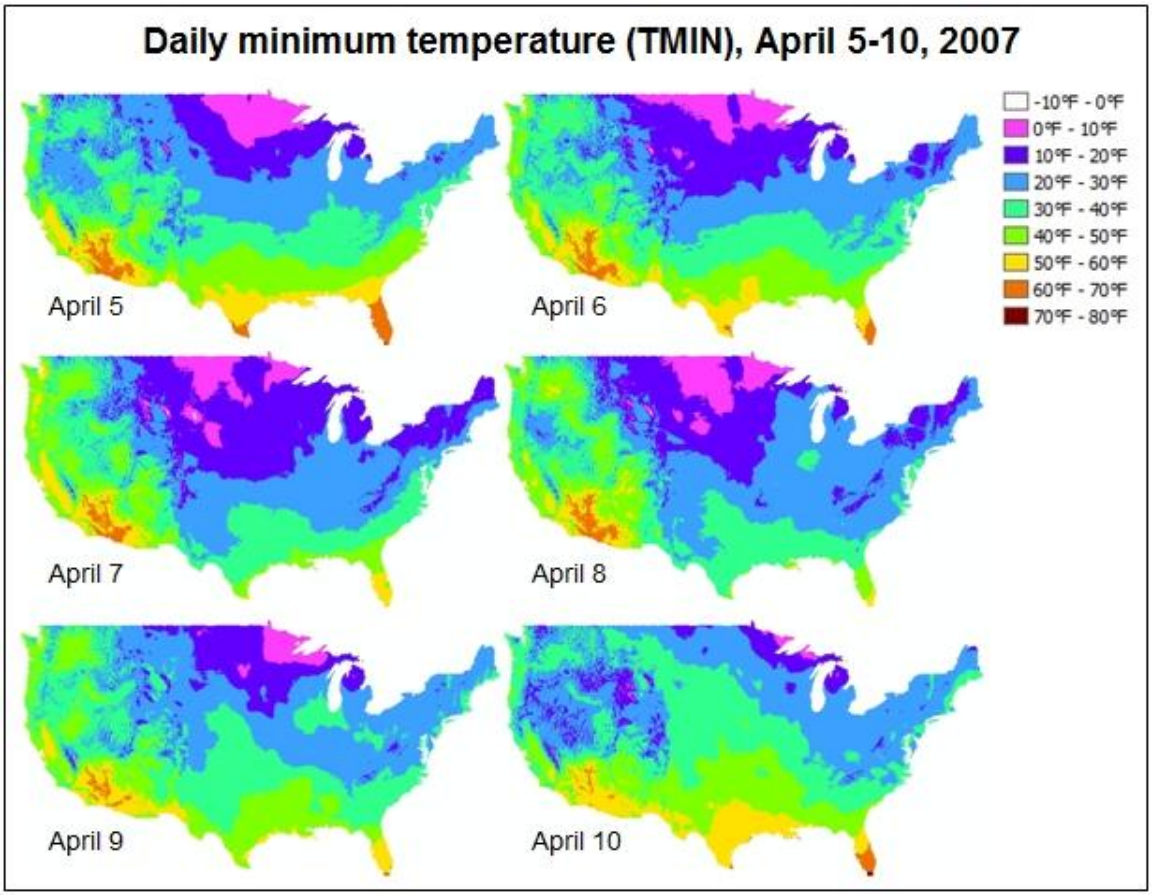

Figure 1-2 Maps showing daily minimum temperature (TMIN) observed during the six-day freeze event, April 5-10, 2007.

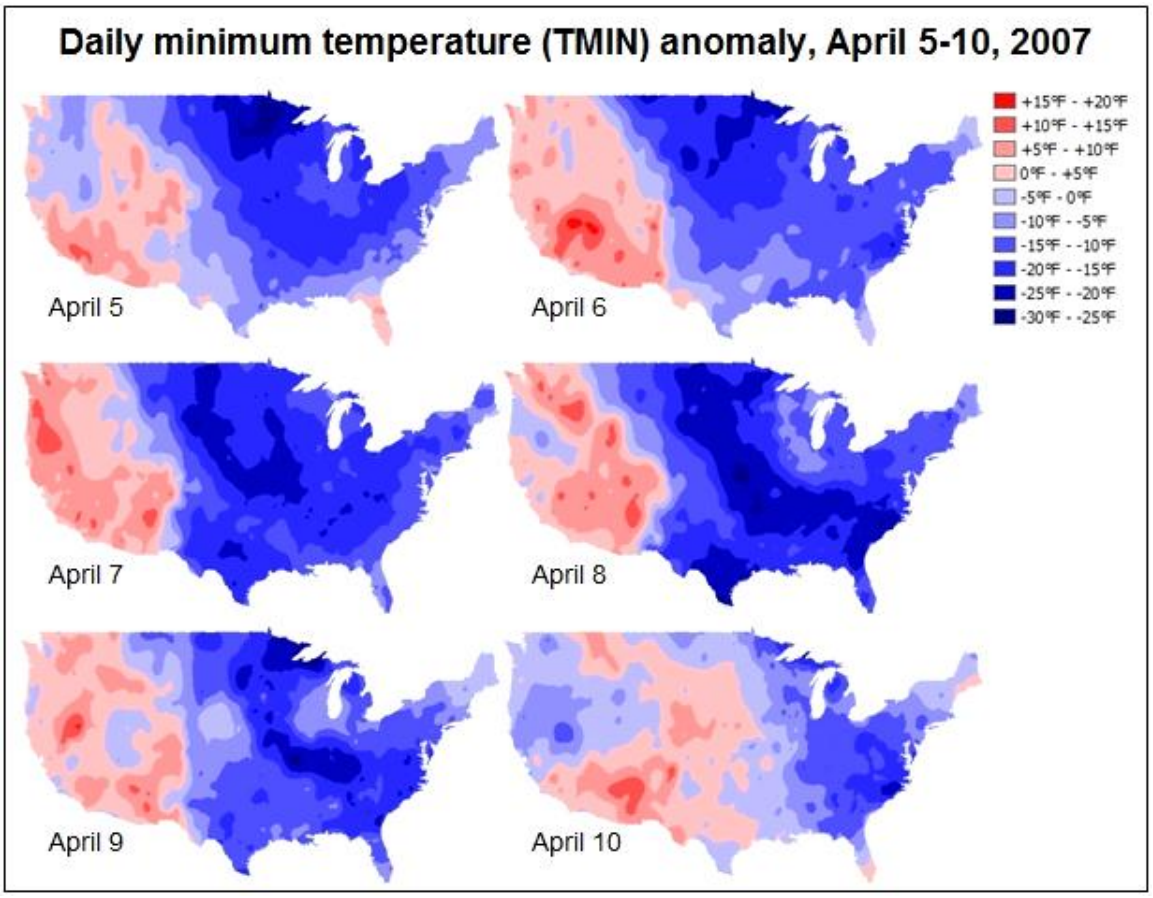

Figure 1-3 Maps showing daily minimum temperature (TMIN) anomaly observed during the six-day freeze event, April 5-10, 2007. Anomaly is based on the observed TMIN value's departure from the normal TMIN for that day.

Although the unusually long duration and record-setting intensity of the April 2007 cold wave made the weather event quite distinctive when considering its climatic context, it did not arrive unusually late in the year, as spring frosts have been known to occur well into May, nor was the geographic extent of its record-setting low temperatures especially unusual, as spring frosts regularly occur throughout the midwest and southeast (Gu, 2008).

Despite this, the freeze was certainly severe enough to cause widespread biophysical effects on the environment, both short-term and long. Depending on several geographic factors such as latitude, elevation, and degree of exposure to sunlight, the new March growth was

stunted, damaged, and in some cases killed off completely by the temperatures sustained during the freeze (Windham, 2008; Mulholland, 2009). The newly formed leaves that had recently sprouted from the bare limbs of thousands of acres of forest became covered in ice and frost before eventually wilting and dying.

While this widespread damage to vegetation was a direct result of the cold temperatures experienced, the unseasonably warm weather that preceded the freeze by weeks must also be considered an instrumental, albeit indirect contributor to the damage. This paradoxical relationship of increased likelihood of freeze damage as a function of increasingly warm early spring temperatures is discussed further in section II-C.

B. Physiological Effects of Frost on Vegetation

To understand the relationship between freeze damage and its effect on the photosynthetic capacity of plant life, it is necessary to possess a clear understanding of the physiological changes that occur, as well as the short-term and long-term consequences of such changes.

The most conspicuous impact is foliar mortality. At the cellular level, frost accumulation causes the formation of ice crystals within and between leaf cells, rupturing cell membranes. Once thawing occurs, rehydration within the cells is restricted and the leaf wilts and dies, shriveling and turning brown in the process (*Fig. 1-4*). Newly formed leaves, buds, and other rapidly differentiating tree tissues have been shown to be the most susceptible to this type of mortality (Inouye, 2000; Oksanen, 2005).

Figure 1-4 Photographs of spring frost damage to various species of deciduous broadleaf trees. Clockwise from top left: Poplar (photo courtesy Utah State University), Walnut (Ontario Ministry of Agriculture), Yellow poplar (University of Tennessee), Red oak (Iowa State University).

Another consequence of a freeze is damage to the apical meristem, the growing tip of a tree that generates leaf buds. The death of an apical meristem can cause the removal of apical dominance, which has consequent effects on tree architecture. For example, with enough frost damage, tree branches might begin to grow laterally instead of from the terminal buds where the dominant meristem is located. Lateral growth inhibits the potential height of the tree, thereby limiting the overall size of the tree canopy and its associated leaf area index, decreasing optimal photosynthetic performance (Paige, 1992).

Among leaves not killed by the frost, injury can be detrimental to canopy health and productivity. Injury can occur in several ways. In non-fatal cases, ice crystals can cause

physical damage to cellular organelles, the most severely impacted of which are the chloroplasts responsible for photosynthesis (Kratsch and Wise 2000). When buds and roots sustain frost damage, often times the damaged portion becomes a site for infection (Haworth and Spiers 1992; Lederer and Seemuller 1992), and once infected, one pathogen often facilitates infection by another (Paul, 1993).

Frosts will freeze the water within stems and branches, producing air bubbles in the ice, a phenomenon known as cavitation. Once the ice thaws, the bubbles are released and block the continuity of water uptake within the xylem, or transport tissue (Sperry, 1992). Deciduous trees have been shown to be particularly susceptible to freeze impacts, since their large conduit volumes make them prone to cavitation and the resultant interruption of the xylem stream. This is especially common following the initiation of new tissue development, which was the case for deciduous forests in March 2007 (Gorsuch, 2002).

Ring-porous deciduous tree species such as oak and hickory have large earlywood vessels located within the youngest growth ring on the outside of the tree, and are produced early in the spring, prior to bud flushing and new leaf development. Because the majority of the tree's water conductance takes place within these nearly-external vessels, the slightest injury to the newest growth ring may immobilize water conductance and force it to use older, less-efficient latewood vessels from the previous years. This contributes to delayed refoliation and can decrease productivity during not only the growth season immediately following the freeze, but the subsequent year's growth season as well (University of Tennessee, 2007).

Tree stress is the major long-term impact that characterizes a severely frost-damaged forest. When newly-formed leaves die as a result of the freeze, the carbohydrate energy the tree had stored up to produce the leaves is essentially wasted. As a mechanism of prevention in case

of such instances, most deciduous trees feature a progressive bud system wherein secondary "backup" buds are available. Trees are then forced to allocate whatever additional carbohydrates remain toward the task of a second refoliation, this time from the secondary buds. As a result, the second refoliation yields lower Leaf Area Index (LAI) due to a sparser tree crown composed of smaller, less dense, and less numerous leaves. Trees are much less productive during the following growing season in this low-energy, "stressed" state (University of Tennessee, 2007).

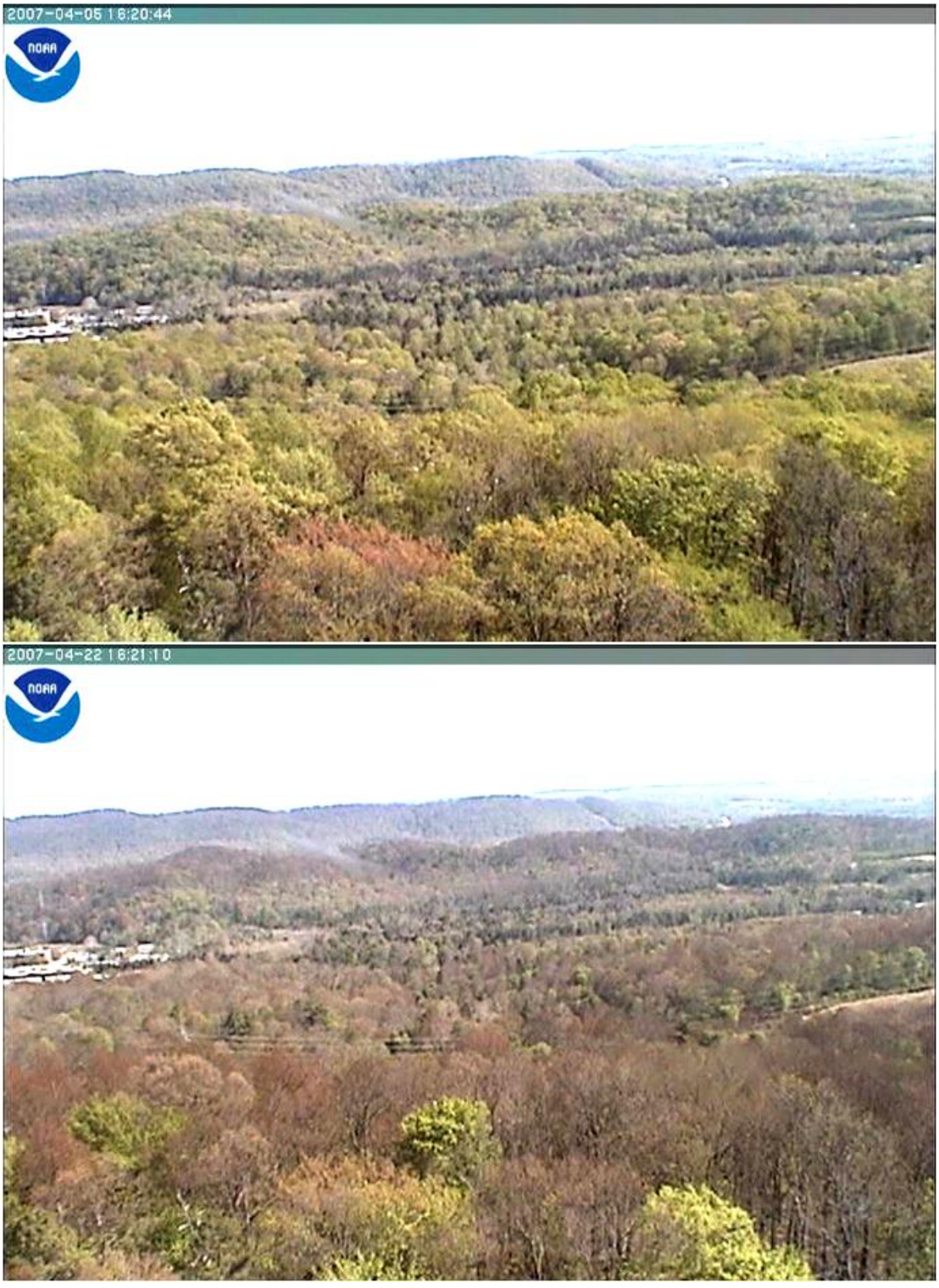

Figure 1-5 Successive photos taken at Oak Ridge, Tennessee on April 5 and April 22, 2007, showing the green, fully-flushed pre-freeze canopy, and the brownness of dead and wilted leaves two weeks later. (ORNL Review, 2007)

C. Research Objective

During weeks of first-hand observations of the damage that occurred throughout the Ozark Mountain region, including wilted plants, flowers, and tree leaves, several questions came to mind. Would all plant and tree species recover from the damage? How long would it take the damaged vegetation to refoliate? Would the re-grown vegetation be as productive as it would have been had it not sustained freeze damage? Would areas that sustained several days' worth of cumulative freeze damage recover at a slower rate than those that experienced only a mild overnight frost?

When thinking critically about geography, one approaches such questions using mental maps. The mental map used to formulate the formal hypothesis of this thesis contained two key themes: the freeze itself, and the biophysical response of the forest to the freeze. Exploratory data analysis using geographic information systems (GIS) led to the focus on whether a spatial "footprint" of reduced forest productivity could be detected within satellite imagery, and, if so, whether it could be determined that an area of decreased productivity was in fact the result of the April 2007 freeze, as opposed to some other environmental stimulus such as a localized drought or an insect infestation.

So, in anticipation of the use of maps to test for the existence of a causal relationship between damaging temperatures and decreased forest productivity, a formal research question was developed, stated as follows: *Are unusually low minimum temperatures sustained during the April 2007 freeze event spatially correlated with unusually low forest productivity observed after the freeze?*

Based on this question, the formal null hypothesis of this thesis was developed. It is stated as follows: *Patterns of unusually-low forest productivity following an April 2007 freeze event are not spatially congruous with the pattern of unusually-low temperatures sustained during the freeze event*. This null hypothesis is designed to test whether or not the spatial characteristics of a map modeling the geographic extent and severity of the April freeze are found in maps modeling abnormally-low forest productivity throughout the remainder of the year.

II. LITERATURE REVIEW

A. Forest Productivity Studies with Remote Sensing Applications

There have been hundreds of studies of forest productivity dynamics employing a remote sensing approach, and although a few of these studies have been concerned primarily with frost impacts, most notably Gu (2008), the majority are not. Of this majority, a common area of research is phenology, the study of climate's influence on the timing of biological phenomena. Many phenology studies using remotely-sensed imagery as a data source have focused on the budburst event (i.e. "leaf flushing" or "leaf-out") that characterizes the onset of the natural spring season.

Examples of these studies include White (1997), who determined a positive correlation between satellite-derived and model-predicted spring onset dates for deciduous forest and other temperate mid-latitude land cover types. Schwartz (1999) performed a similar study, finding that when compared to an average of all landcover types, deciduous forest had a more positive correlation between the model and NDVI observations of spring onset. Jenkins (2002) studied phenology by calibrating temperature data with NDVI imagery over an 11-year period, revealing a relationship between remotely-sensed spring budburst and the accumulation of temperature-based forcing units that regulate it. Chen (2005) used MODIS vegetation index products to test its detection of reduced productivity among several boreal forests at different stages of wildfire recovery, finding them to be "useful for interpreting and mapping surface vegetation representing various temporal states of disturbance across broad areas." Ahl (2006) recorded deciduous canopy green-up with *in-situ* measurements of FPAR and Leaf Area Index, and compared them with that of MODIS vegetation indices, finding no significant discrepancies between values obtained by the two methods; Houborg (2007) further explored the

understanding of benefits obtained by combining satellite-derived vegetation indices and field-based approaches to determining physiological parameters such as LAI, FPAR, and total vegetation water content.

B. Forest Productivity Studies with Other Applications

Conversely, frost impacts on deciduous forest productivity have been studied extensively, but in most all cases by using an approach other than that involving remotely-sensed satellite imagery. The most common alternate methodology has been the use of computer simulation forest growth modeling (Kellomaki, 1995; Kramer, 1996; Kramer, 2000; Raulier and Bernier, 2000; Hanninen, 2006). Others have included measurements of stomatal and hydraulic conductance in a laboratory environment (Gorsuch, 2002), tree-ring analysis (Dittmar, 2006), qualitative observation (Zasada, 1999), and *in-situ* measurements of PAR and stream water chemistry via quantum sensor and nitrate/nitrite sampling (Mulholland, 2009).

Most recently within this category, Awaya (2009) used field measurements of LAI and NPP over a four-year period following a significant April 2001 frost that killed 80% of newly-formed leaves at a beech forest stand in northern Japan. The frost was preceded by two weeks of warmer-than-average April temperatures, mirroring the meteorological conditions from 2007 of interest to this thesis. After analysis of his data, Awaya found that forest productivity was "greatly reduced" during the 2001 growing season, with PAR falling more than 50% from the averages of the previous two years, and LAI decreasing to 30% of its normal annual values. However, the post-freeze "latent" leaves that grew from backup buds were found to have thrived in the abundant radiation produced by a thinner forest canopy lacking its normal amount of growth-suppressing shadow. So, while throughout the 2001 growing season there were less

leaves present, and less productivity overall, the loss was somewhat compensated for by the increased exposure to sunlight that allowed the post-freeze growth of latent leaves to be 1.7 times more productive than the primary leaves of other years.

C. Spring Frosts and Climate Change

While concluding his article, Awaya (2009) references the relationship between spring frosts and climate change, stating that the risk of spring frost damage would *decrease* given the increasing average annual air temperatures associated with global warming. However, Awaya was certainly not the first researcher to breach this topic. Much of the research done to analyze the impacts of spring frost on forests has addressed this suggested association with climate change, and Awaya's findings conflict with decades' worth of previously-drawn conclusions.

In one of the earliest articles to focus on spring frosts in the context of climate change, Cannell (1986) observed a warming trend in 20th century Britain and found that if the trend were to continue, future warming within temperate climates would induce earlier budburst in trees without a corresponding decrease in the frequency of spring frosts. The earlier budburst, Cannell proposed, would leave new growth susceptible to frost and lead to an increase in post-budburst frost damage.

Hanninen's research (1991) on boreal-zone hardwood trees supported this theory, finding that they would suffer "substantial" frost damage even under "slight" climatic warming. Hanninen explained how climate change's alteration of the coordination between photoperiod and thermal regime can produce adverse effects on tree performance by causing premature onset of growth following mild winters. Kramer (2000) provided evidence to support Hanninen's conclusions, but differentiated between the effects of spring frost to boreal-zone and temperate-

zone trees, concluding that their differences in response to climate warming are due to their different hardiness factors – that is, that temperate-zone trees are typically in a different state of "chilling" by the end of the winter than are boreal-zone trees. In doing so, Kramer suggested that the trend toward earlier dates of boreal budburst, and therefore the increase in frost damage risk, was less than predicted by Hanninen's model.

Menzel and Fabian (1999) constructed a model for simulating the consequences of climate change on the spring phenology of temperate Europe, finding that "the onset of spring events is sensitive to climatic change and will advance by up to six days per 1 °C increase in winter air temperature, depending on the species." Referencing Menzel and Fabian's results, Inouye (2000) concluded that "the recently documented increase in the length of the growing season in Europe is one indication of a change that may result in more frequent spring frost damage to plants."

That same year, Linkosalo (2000) analyzed two different models for predicting changes in phenology as a result of a warming climate; one based on the accumulation of chilling temperatures, and another also accounting for the accumulation of light units. Linkosalo found that "estimates of frost damage risk with simulated climate change differed radically between the two models," concluding that "our current knowledge of spring phenology is not a sufficient basis for reliable forecasts" and stressing the need for further understanding of how to properly model the cooperation between climatic factors and biophysical mechanisms. However, Linkosalo's models agreed that an increased risk of damage to deciduous trees of Europe could be expected as climate change induces an earlier onset of spring.

Seemingly in agreement with Linkosalo is Mulholland (1999). At Oak Ridge, Tennessee, much nearer to the geographical focus of this study than Europe, Mulholland analyzed the last

half-century of climate data (1950 to 2007) and observed that the late winter period had become increasingly warmer. In fact, March 2007 was found to be Oak Ridge's warmest March on record. Interestingly, however, no year-to-year trend in the annual occurrence of the last hard freeze was found, and the April 2007 freeze was not unusually late. The annual dates of the last hard freeze were found to be highly variable, suggesting that late spring freezes of the timing and magnitude of April 2007's may become more common given future climate warming.

Perhaps the most comprehensive study of the freeze's implications for climate change was authored by Gu (2008). After the Easter 2007 freeze, Gu obtained MODIS NDVI imagery of the affected region depicting what he described as a late-April "green retreat" of high-productivity vegetative development that had reached as far north as northern Missouri. The retreat, wherein the "vernal front" of productivity was pushed back to the lower latitudes of the Deep South, stood in stark contrast to conditions at the same time during the previous year, when late-April greenness had already spread as far north as the Great Lakes region. Referencing the Missouri Ozark AmeriFlux site's recording of reduced forest carbon uptake and altered surface energy balance (Gu et al., 2006), in addition to markedly lower readings of regional post-freeze PAR, Gu expressed reason to believe that the frost damage incurred may have profound impacts on the terrestrial carbon cycle of central and eastern United States.

By all accounts, the carbon balance had indeed been significantly altered by the freeze. Typically, by early May, forests in the region would be near peak photosynthetic productivity, carbon fixation (CO_2 uptake driven by forest respiration) would be near an annual maximum, and a negative carbon flux, indicative of a healthy forest, would be achieved. However, on May 3, 2007 the NOAA reported above-average CO_2 levels throughout the Mid-South (NOAA, 2007). This indicated that by this point in the spring season, vegetation had failed to create a terrestrial

carbon sink. Forests had not yet achieved a collective respiration rate sufficient to produce the oxygen necessary to offset the rate of CO_2 produced by human and animal life.

Whether or not such increased atmospheric CO_2 is a direct consequence of frost damage, studies have proven that over the long-term, it may lead to further frost damage. Elevated CO_2 levels have been shown to reduce plant tolerance of freezing temperatures (Loveys 2006), and it may increase foliar ice nucleation temperatures in deciduous species, leaving them vulnerable to merely moderate cold (Beerling 2001). Furthermore, elevated CO_2 was found to promote spring frost damage after two weeks of mild early spring temperatures (Lutze, 1998). Given the IPCC's prediction of a doubling of atmospheric CO_2 by the year 2100, such effects are particularly profound with regard to the future health of forests (Watson, 2001).

In theory, this impact to the terrestrial carbon balance could have long-term ramifications. Exacerbation of the climate change process is one such effect. If left susceptible to frost damage, biophysical alterations to tree physiology can limit the annual respiration rate of an entire forest stand. This rate represents carbon fixation, which plays a significant role in the global carbon cycle, itself a key driver of global warming. Therefore, if it can be determined that spring frost damage can alter the rate of carbon fixation, even on a merely regional scale, then adjustments to the global climate change models that account for such influences must be made accordingly.

III. METHODOLOGY

The methodology designed for this research project may be summarized by the following steps: 1) Use surface temperature data to create a freeze map that models the severity of the April 5-10, 2007 freeze event by showing where and to what degree potentially damaging minimum temperatures were sustained. 2) Use satellite imagery to create maps modeling forest productivity throughout 2007, including maps of productivity as observed prior to and following the freeze event.

Once the freeze map and forest productivity maps had been processed, the objective was to analyze their patterns for spatial congruence. To accomplish this, the following steps were taken: 3) Create a "product" dataset featuring values derived from the product, or multiplication of, freeze map values and forest productivity map values. 4) Calculate Moran's I coefficients in order to summarize the spatial autocorrelation of rasters from the forest productivity set and product set. Finally, 5) compare Moran's I coefficients of rasters in the forest productivity set with those of rasters in the product set.

Study Area

The April 2007 cold wave affected a large portion of the contiguous United States, so the full spatial scale of the phenomenon being studied can be said to encompass the Midwest, southern plains, and Southeast, generally speaking. However, this research focuses on a narrower geographic range defined precisely as the boundaries of the MODIS imagery "tile" used for modeling forest productivity response (*Fig. 3-1*; the MODIS data product is described in greater detail in section III-B). This tile includes the entirety of Arkansas, Mississippi, and Alabama, plus most of Missouri, Kansas, and Louisiana, and significant portions of Oklahoma,

Tennessee, and Georgia. Although the single tile does not represent the full geographic scale of the freeze event, it was selected as the data frame for the following reasons. For one, the study initially intended to focus on the Ozark Plateau region surrounding Fayetteville, Arkansas, where freeze impacts were observed firsthand. The tile ultimately chosen features complete coverage of the Ozarks, and was therefore a suitable choice. Another reason was manageability; the imagery contains a fairly large amount of information and therefore large file sizes, so a smaller, single-tile data frame would be much easier to manage than would multiple tiles, especially when working with a time-series data set involving dozens of processing steps.

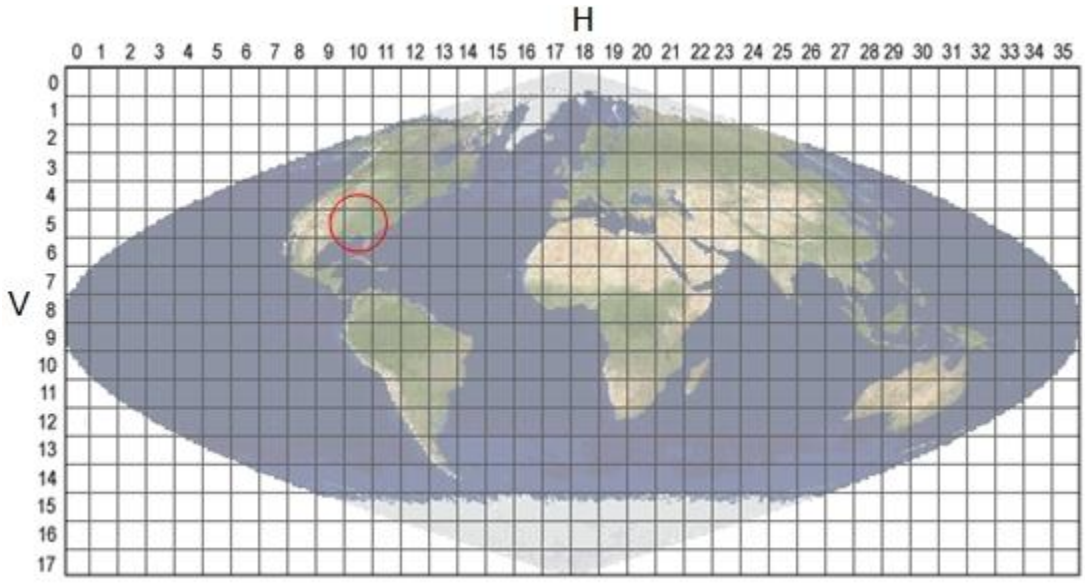

Figure 3-1 The MODIS sinusoidal grid shows the format that NASA uses for publishing its imagery in individual files known as "tiles." The specific tile used for this study, H10 V5, shown circled in red, occupies 30-40° north latitude, and -104.42° to -80.83° west longitude.

Use of anomaly data

To create the freeze map and forest productivity maps, the raw data was required to be processed in various ways. Some of the processing was necessary in order to address technical issues related to formatting and compatibility, but the majority was done to create anomaly datasets. Because of the spatio-temporal nature of this study – the way data is analyzed over space and time – anomaly data was needed to understand the observed values in their geographic and seasonal contexts.

Using anomaly to consider the geographic and seasonal contexts of observations helps control for the effects of spatio-temporal variability when a geographic study employs time series data, as does this particular study. Phenology, or the seasonal timing of naturally occurring phenomenon, e.g. spring budburst, is a good example of how spatio-temporal variability affects this study. Budburst is a spring occurrence in the temperate climates of the United States interior, but it features a prominent spatio-temporal aspect; for example, deciduous trees of the Gulf Coast region put out new leaves weeks prior to those near the Great Lakes.

Given the relationship between distance and biophysical diversity, it is worth considering the 550,000 square miles of land surface represented by the satellite imagery used in this study, and the potential within it for disparity among climates and the vegetation types they support. Because of these regional climate differences, spring freezes occur more frequently to the north than they do to the south. Additionally, deciduous forest tree species native to the relatively-colder climates of the north possess a certain hardiness that more adequately protects them from spring freeze damage than do that of forest species occupying the relatively-warmer climates to the south. It follows, then, that during a spring freeze event, a particular duration and quantity of freezing temperatures would induce more damage to forests of the south than it would to forests

of the north. In other words, potentially damaging temperatures vary by location, generally as function of latitude.

Therefore, due to the geographic component inherent in the damage potential of minimum temperatures, and the damage response of forest productivity, it was determined that the maps used for analysis should not feature direct observations, but their anomaly counterparts instead. By using anomaly values, the observations are "standardized" across both space and time. Variables such as tree species hardiness, and the likelihood of frosts occurring at any given place and time, are controlled. Most importantly, temperature map values more accurately model potential damage, and forest productivity maps more accurately model any apparent reaction to that damage.

To create the anomaly data, observations were required of surface temperature and forest productivity values for April 5-10, 2007 specifically, as well as observations for the dates of April 5-10 throughout previous years. By taking the average of as many observations from previous years as possible, daily normal values could be created. These daily normals could then be used as a baseline by which to determine the degree of deviation from them by the 2007 observed values. This degree of deviation, or departure from normal, is represented by the anomaly data.

A. Surface Temperature Data (Freeze Map)

To model the potential damage of the April 5-10, 2007 cold wave and show where and to what degree potentially damaging temperatures were sustained, a freeze map in raster format needed to be created. The map was originally conceived of as depicting the total accumulation of temperature measurements for the duration of the weather event. Ideally, the temperature measurements would have been recorded at the smallest possible time interval, i.e. hourly, or

even by the minute. Unfortunately, sources for georeferenced raster-format weather data are limited, and the finest temporal resolution among available data was at the daily scale. This data was obtained from NASA's Ecological Forecasting System (ECOCAST) program, which draws from over 1,400 National Weather Service stations to produce raster files of observational and historical climate data, including surface air temperatures of the continental U.S. at a spatial resolution of 8 kilometers per pixel (Nemani, 2005). The observation type chosen was daily minimum temperature (TMIN), the minimum temperature observed over a 24-hour period. In total, twelve of these raster files were obtained: six daily TMIN rasters corresponding to the six-day period of April 5-10, 2007, and six daily normal TMIN rasters, featuring values representative of a 30-year historical average based on the years 1970-2000.

Processing the freeze map involved the use of map algebra, a GIS tool for applying arithmetic functions to multiple rasters on a per-pixel basis (the tool was also used in processing the EVI imagery, as explained in the following section). Using a function for subtraction, a set of six daily TMIN anomaly rasters were created by calculating the difference between each of the six daily observed 2007 TMIN rasters and its associated daily normal. Then, using the map algebra tool for addition, the TMIN anomaly rasters were summed to produce a single cumulative TMIN anomaly raster (*Fig. 3-2*) depicting the total six-day accumulation of TMIN anomaly during April 5-10, 2007.

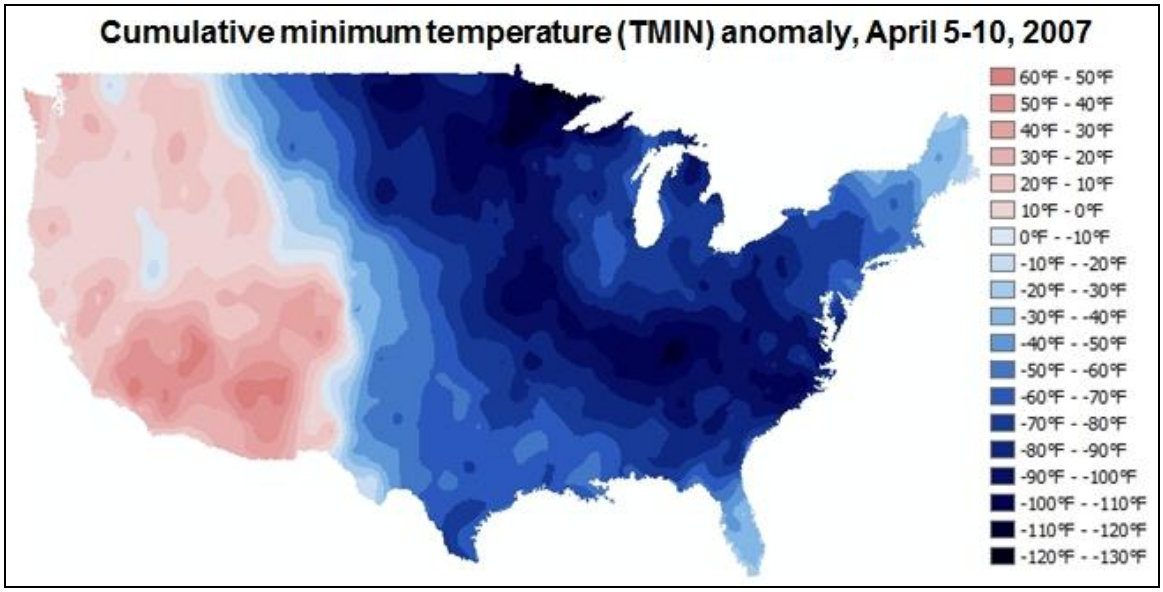

Figure 3-2 Featuring values derived from an arithmetic sum of the values of the six daily TMIN anomaly maps in *Figure 1-3*, the greatest accumulation of anomalously-low TMIN, shown here in dark blue, represents the greatest degree of potential freeze damage to deciduous forests.

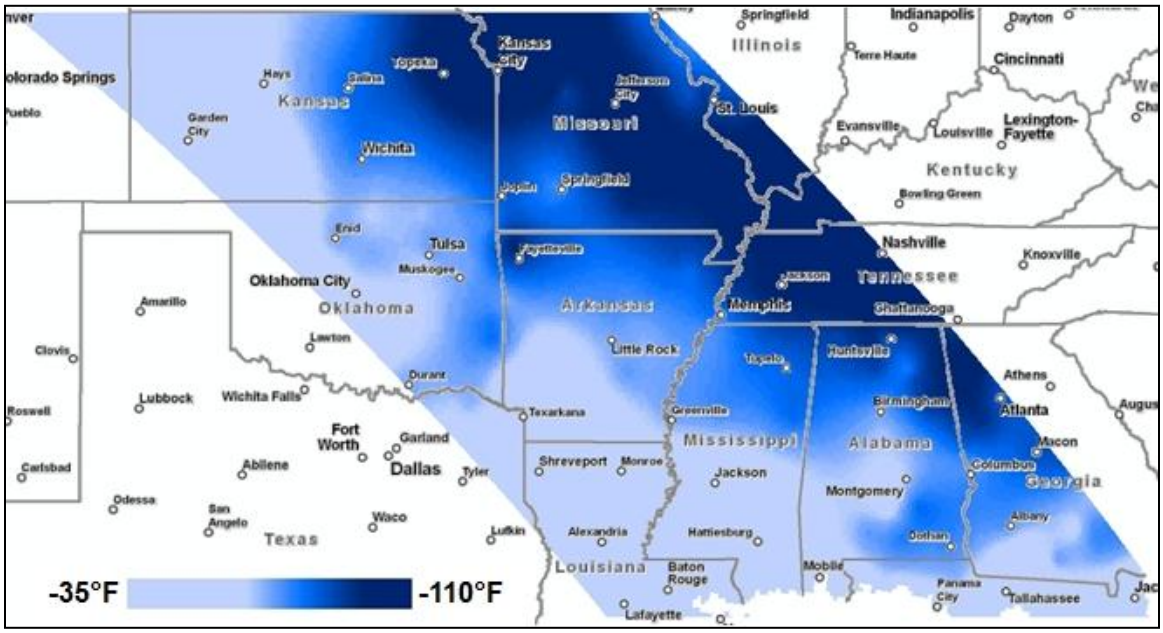

Figure 3-3 Cumulative TMIN anomaly from *Figure 3-2* is shown here cropped to the spatial extent of the MODIS imagery used for analysis. The color ramp used for value visualization in this map assigns dark blue to locations with the greatest accumulation of degrees below normal (and therefore the highest potential for freeze damage to deciduous forests).

B. EVI Data (Productivity Maps)

For creating maps to model vegetative productivity, remotely-sensed satellite imagery was used. Unlike traditional color photography, in which images are based on the surface reflectance of various wavelengths within the portion of the light spectrum visible to the human eye, NASA's Moderate Resolution Imaging Spectroradiometer (MODIS) satellite sensor produces images based on the reflectance of wavelengths that occupy a wider spectrum, including non-visible portions. This wider light spectrum is divided into sections that are recorded as spectral bands. MODIS produces images at 36 spectral bands, ranging from wavelengths as small as 620 nanometers to as large as 14,385 nanometers. MODIS makes daily observations and NASA publishes the imagery, fully georeferenced, as 16-day composite images (Huete, 2002).

While imagery can be generated from individual bands, scientists use an algorithm to combine multiple bands into a vegetation index, a data product that highlights terrestrial vegetation's capacity for photosynthetic productivity by way of its chlorophyll content. The Normalized Difference Vegetation Index (NDVI) and Enhanced Vegetation Index (EVI) are two of the most frequently used. EVI, the index used for this research, is an optimized version of NDVI developed by MODIS engineers specifically for the MODIS platform. Its advantages include improved sensitivity in high biomass areas like forests, and reduced atmospheric noise through the use of a blue band to correct for the influence of aerosol scattering.

EVI is useful for modeling Net Primary Productivity (NPP), or the rate of photosynthesis, so it can be thought of as an indicator of vegetative health. EVI value is a function of several biophysical variables detected by the MODIS sensor. These variables include measurements of reflectance at the red (645 nm) and near-infrared (858 nm) wavelengths of Photosynthetically

Active Radiation (PAR) absorbed by the canopy, as well as measurements of blue (469 nm) wavelength reflectance. These three specific wavelengths in particular are employed because of their instrumental roles in photosynthesis; light energy is absorbed by the chlorophyll contained within the leaf's palisade mesophyll layer at the blue and red wavelengths, and it is reflected and scattered by the leaf's spongy mesophyll layer at the near-infrared wavelength.

EVI values occupy a scale ranging between a maximum of 10,000 (absolute optimal productivity) to a minimum of -3000 (productivity non-existent, technically counter-productive). To calculate these values, the aforementioned red, blue, and near-infrared reflectance values are input as variables in the following equation:

$$EVI = G \frac{NIR - RED}{NIR + (C_1)RED - (C_2)BLUE + L} (1 + L)$$

Where the coefficient *G* is a gain factor set to 2.5, *L* is a soil adjustment factor of 1.0, and C_1 and C_2 correspond to the use of the blue band in correction of the red band for atmospheric aerosol scattering, with values of 6.0 and 7.5, respectively (Huete, 2002). As a means of data validation and quality control, EVI values for a target site are coupled with that site's corresponding Leaf Area Index (LAI) value, an indicator of biomass defined as the total one-sided green leaf area per unit ground-surface area (Jensen, 2005).

The imagery obtained is recorded by NASA's Terra (EOS AM-1) and Aqua (EOS PM-1) satellites at a spatial resolution of 250 meters, the surface distance width represented per pixel. The two satellites share the same orbit around the Earth, yet they are fixed in diametrically-opposed positions relative to one another. Although their images are released every 16 days as composites formed from 16 individual daily observations, the dual-satellite arrangement allows for a phased production schedule wherein an image from either satellite is produced every eight

days. For example, the 16-day production period for Terra would begin on day 1, which corresponds with day 9 of Aqua's 16-day period. A set of thirty EVI images was ultimately obtained, spanning March 8 to October 24, in order to represent the phenological growing season from budburst to autumn senescence.

In order to generate daily normals that were as robust as possible – that is, comprised of as many years' worth of available daily observations available – images corresponding to these thirty days were originally obtained from all years of MODIS's operation, from 2000 to 2007. However, because the Aqua satellite did not begin operating until July 4, 2002, more than two years after Terra on February 24, 2000, only the annual datasets in which the phased production schedule of the dual-satellite system was available were used for this research, and the Terra-only datasets recorded prior to the 2003 growing season were omitted. This way, each daily normal in the normals set would be based on the same four years' worth of EVI values (2003-2006), keeping each of the 30 daily normals equally robust throughout the entire dataset.

For processing the five years' worth of raw MODIS EVI raster data obtained (30 days per year, 2003-2007), the objective was to create two different types of annual time-series EVI sets: a set of daily EVI normals, featuring the arithmetic means of daily values observed between 2003 and 2006, and a set of daily EVI anomalies, featuring the daily departure from normal of the values observed in 2007. Processing would have been a much simpler task had the raw data values been thoroughly accurate. However, because the accuracy of MODIS data products often suffers from atmospheric interference, imagery from certain storm-prone days can return poor-quality data in the form of questionable pixel values. Because NASA publishes its imagery with the unreliable pixels intact, it is necessary to first remove them before continuing with any further processing.

Removal of the unreliable pixels, or "cleaning" of the imagery, was accomplished using pixel reliability rasters that are included with the multi-band MODIS data product file published by NASA. The imagery raster and the reliability raster are separate, but maintain a spatial association; they possess the same dimensions and resolution as one another so that the same pixel from either raster represents a single location on the Earth's surface. Essentially, the reliability raster is an indicator of the usefulness of EVI raster values, per-pixel. Reliability pixel values are coded as either -1 (meaning "fill/NoData"), 0 ("good data"), 1 ("marginal data"), 2 ("bad data - snow or ice cover"), or 3 ("bad data - cloud cover"), and these codes are based on surface conditions as determined by NASA via their own *in situ* validation efforts.

Using the spatial analyst tools available within ESRI ArcGIS software, the first step of processing was to convert the pixel values of the 150 reliability rasters (5 annual sets of 30 daily images per set). Reliable pixels coded 0 and 1 ("good" and "marginal" data) were both converted to a value of 1, where pixels coded with any other value ("fill/NoData," "snow/ice," or "cloudy") were converted to a placeholder (non-integer) value of NoData. Then, using a GIS tool (extract by mask), each of the 150 EVI rasters were extracted by a mask of its corresponding reliability raster. This produced an output set of 150 'clean' EVI images in which pixels formerly designated as unreliable were effectively removed by being assigned a value of NoData.

With the reliability rasters and EVI rasters now clean, the EVI normals set could be processed. Using map algebra function for addition, the four years' worth of daily reliability rasters were summed. Output result was a set of 30 daily cumulative reliability rasters, each consisting of values ranging between 0-4 to indicate the number of years' worth of available EVI values (2003-2006) contributing to the mean EVI value for each individual pixel on a particular

day. The same method was then used to sum four years' worth of EVI rasters and produce a set of 30 daily cumulative EVI rasters.

Finally, to produce the set of normals, each of the 30 cumulative EVI rasters was simply divided by its corresponding cumulative reliability raster. Once the normals had been created, the anomaly set could be processed by using a subtraction function to calculate the difference between each daily normal and its corresponding 2007 raster.

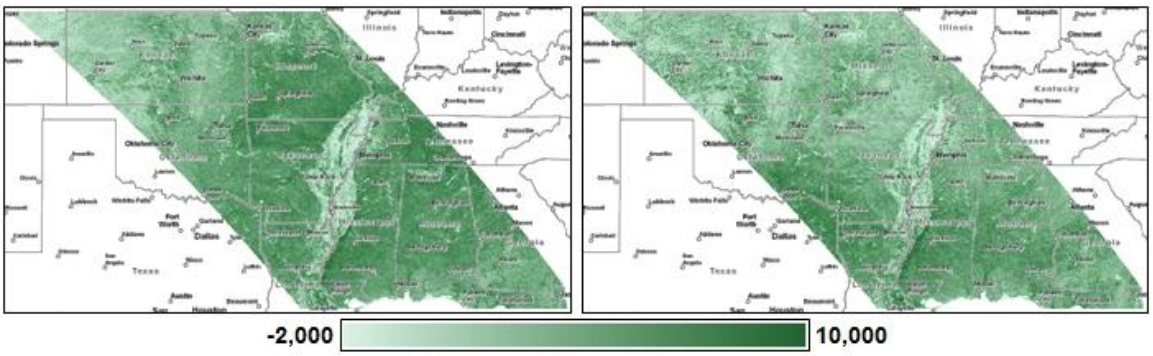

Figure 3-4 Imagery on the left shows normal EVI values for April 23rd, whereas the imagery on the right shows EVI values as observed on April 23rd, 2007, two weeks after the freeze event. The green-scale color ramp uses dark green to depict the higher values representative of greater vegetative productivity.

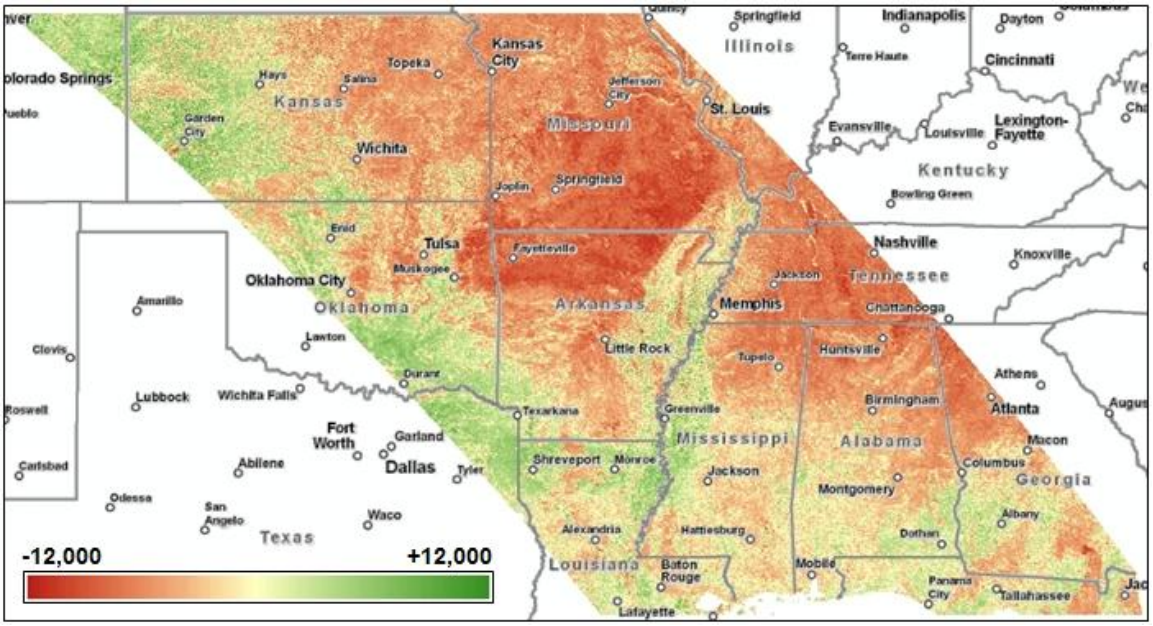

Figure 3-5 The difference in productivity apparent in *Figure 3-4* is shown here highlighted as the EVI anomaly imagery for April 23rd, 2007, two weeks after the freeze event. The color ramp used for visualization depicts areas of unusually low vegetative productivity as red, areas of unusually high productivity as green, and areas featuring no significant change as yellow.

C. Product Data (Freeze Map × Productivity Maps)

The "product" dataset was created as a way to interpret the freeze map and vegetation productivity maps together using descriptive statistics, as explained later. It is composed quite literally of products, meaning that its values are generated by a map algebra function that multiplies freeze map values by EVI anomaly values. Before they could be multiplied together, however, the contributing values of the freeze map and EVI anomaly rasters needed to be re-scaled to a common range.

Once the freeze map had been cropped to occupy the spatial extent of the EVI imagery (*Fig. 3-3)*, it contained values ranging between a cumulative minimum of -110.52°F and a cumulative maximum of -34.92°F. Since the minimum temperature value represented the maximum potential damage, and vice versa, these values were reclassified to a new 100-class range featuring a maximum of 100 and a minimum of 1, respectively.

The EVI anomaly rasters were also scaled to this 100-class range, although their reclassification technique was different, since all 30 rasters in the set had their own individual minimum and maximum values. To reclassify them, all positive anomaly values were first converted to a value of 1. This automatically classified any positive anomaly values as the lowest possible value on the new scale, since the new scale is designed to indicate damage response in the form of decreased vegetative productivity, and positive anomaly values cannot possibly represent decreased vegetative productivity. The remaining population now consisted of entirely negative anomaly values. These were reclassified by assigning the lowest negative anomaly value from the entire set of 30 rasters (-11130, the "global" minimum, featured in the imagery for day 177) as the new maximum of 100, since it represented the maximum damage response observed. Negative anomaly values from all rasters were then reclassified to a 100-

class range featuring a maximum of 100 and a minimum of 1. The actual map algebra function that multiplied freeze map and productivity map values together is contained within the sampling step, as explained in the following section.

D. Sampling

The GIS tool that calculates spatial autocorrelation is designed to work on vector format data exclusively. Unlike the raster format, which organizes spatial data in a grid, the vector format organizes its files using a coordinate-based system of feature class points. Essentially, points are to the vector format what cells, or pixels, are to the raster format. Although it would have been possible to simply convert the freeze map and EVI imagery from raster to vector format, it would not have been practical, since the calculation of spatial autocorrelation for a single vector file with 5,000 points requires approximately two hours of computer processing time. When considering that there are 60 rasters for which to calculate Moran's I, and the total pixel count – and therefore the potential point count – exceeds one million for each, it was obvious that the data volume needed to be reduced through sampling.

Were pixels to be randomly sampled from the millions of pixels comprising the freeze map or any given EVI image, the sample would likely represent a variety of different land cover types. This was problematic, since this study focuses on the correlation between freezing temperatures and the productivity of a specific land cover type, deciduous broadleaf forest. Pixels representative of other land cover types where productivity is not as susceptible to freeze damage, e.g., evergreen forest, prairie, cropland, or water bodies, were considered undesirable data and needed to be excluded from the sample. Furthermore, to insure that the exact same pixels were being sampled throughout every EVI raster in the set of 30, unreliable pixels that had

been previously removed through cleaning in as few as one needed to be restricted from all the rasters in the set in order to prevent any of them being sampled. With these requirements in mind, a sampling technique was designed to isolate pixels consistently reliable throughout the entire set, isolate the target land cover type, and then randomly select no more than 5,000 pixels from the mutual population defined by the first two criteria.

To isolate the valid pixels, all 30 EVI images from 2007 were summed together using map algebra. Since the output of map algebra functions always feature NoData values where any of the input rasters did, the valid pixels in the EVI sum raster represented the only pixels that were consistently reliable throughout the entire 2007 set.

Next, to isolate the deciduous broadleaf forest land cover type, a data product was obtained that classifies each and every pixel featured in the EVI imagery as one of several discrete land cover types. NASA's MCD12Q1 data product, conveniently derived from the same MODIS satellite sensors that produce the EVI imagery, provides such a classification scheme. After obtaining the data product and converting it to raster format, the land cover type of interest, deciduous broadleaf forest, was isolated from the twelve other land cover types. It was then filtered by a mask of the valid pixel raster, creating an output raster containing valid, deciduous broadleaf pixels.

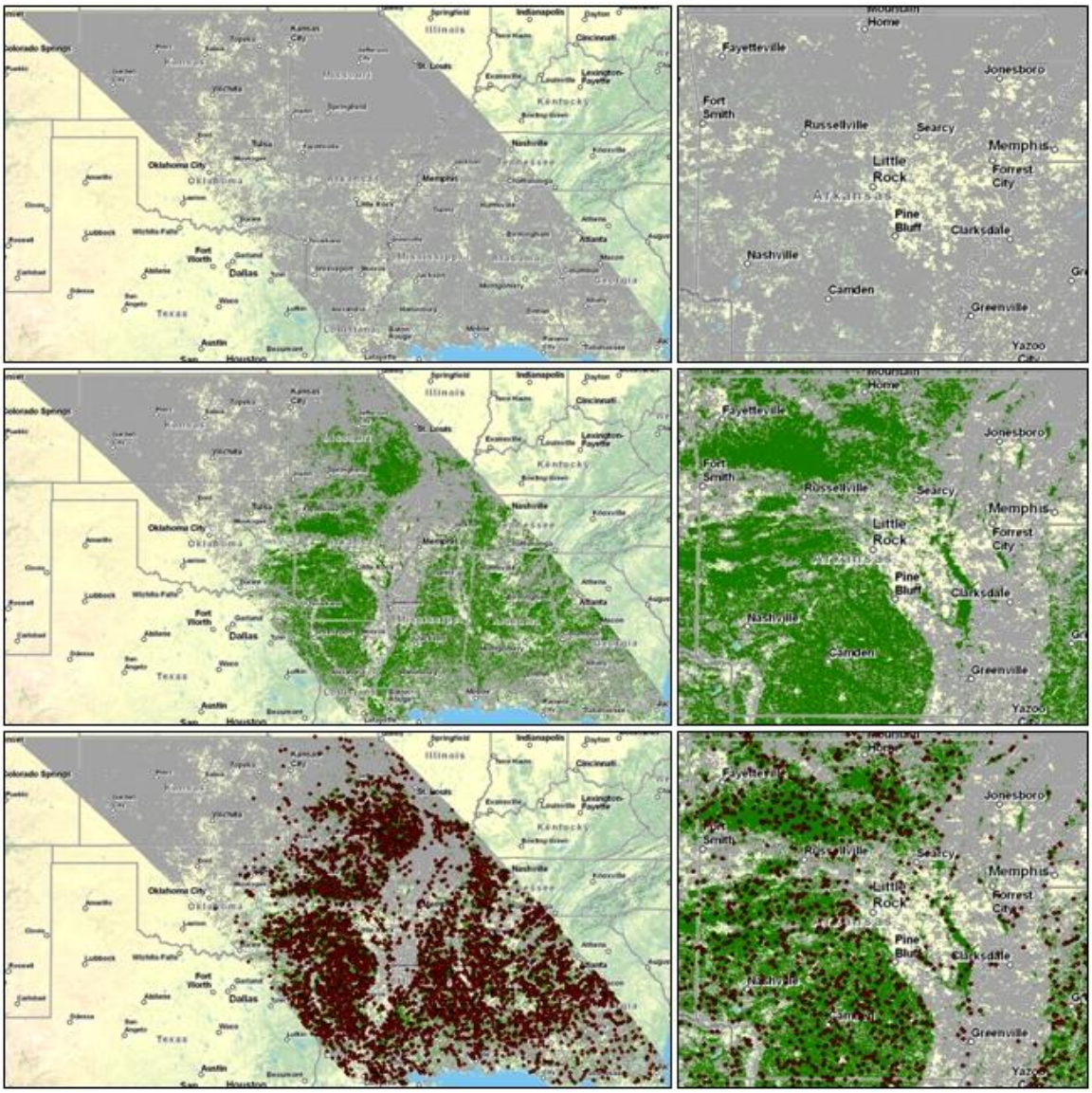

Figure 3-6 Maps showing the various layers associated with the sample site selection process, with the full extent of the MODIS tile shown in the left-hand column, and a detail of Arkansas to the right. In the top row, a composite of the 2007 EVI imagery set reveals where pixels were valid throughout all 30 images, and where pixels unreliable in as few as one have been removed. Overlaid atop this layer, in the middle row, is the deciduous broadleaf forest land cover class in green. The map on the bottom row features 5,000 sample site points overlaid atop the previous two layers from which they are selected.

Then, using a GIS-based tool for random raster generation, a raster was created featuring pixel values consisting of random decimals distributed uniformly within a range of 0.0 to 1.0.

The values were carried out to six decimal places (i.e. 0.683412), and the tool was provided with an EVI image as a template so that the random raster output would possess its same dimensions and resolution. This random numeral raster was then filtered by a mask of the valid, deciduous broadleaf pixel raster, producing an output raster of valid, deciduous broadleaf pixels containing random values. The total pixel population of this raster was 4,891,845, so a reduction to 0.001022% of the original size was necessary to produce the desired sample size of 5,000 pixels. This reduction was achieved by reclassifying all values less than 0.001022 to 1, and all values greater than 0.001022 to NoData. The raster now contained 5,000 valid, deciduous broadleaf pixels acting as the sample sites (*Fig. 3-6).*

To create the sample sets, the 5,000-pixel sample site raster was used as a mask by which to select pixels from the freeze map and the EVI anomaly rasters, thereby "sampling" them. The anomaly sample rasters were then converted to vector format (*Fig. 3-7*). To create the product raster set sample, the sampled EVI anomaly raster pixels were simply multiplied by the freeze map and converted to vector (*Fig. 3-8*). This method precludes creation of a set of "full" product raster files in lieu of a set of samples. Processing a set of full product rasters would only have been necessary as a means for ultimately procuring a sample, so by using this more efficient method, redundant steps are circumvented, with no loss of data integrity. The minimum, maximum, and mean values of both the EVI anomaly sample set and the product sample set are listed in Table 4-1.

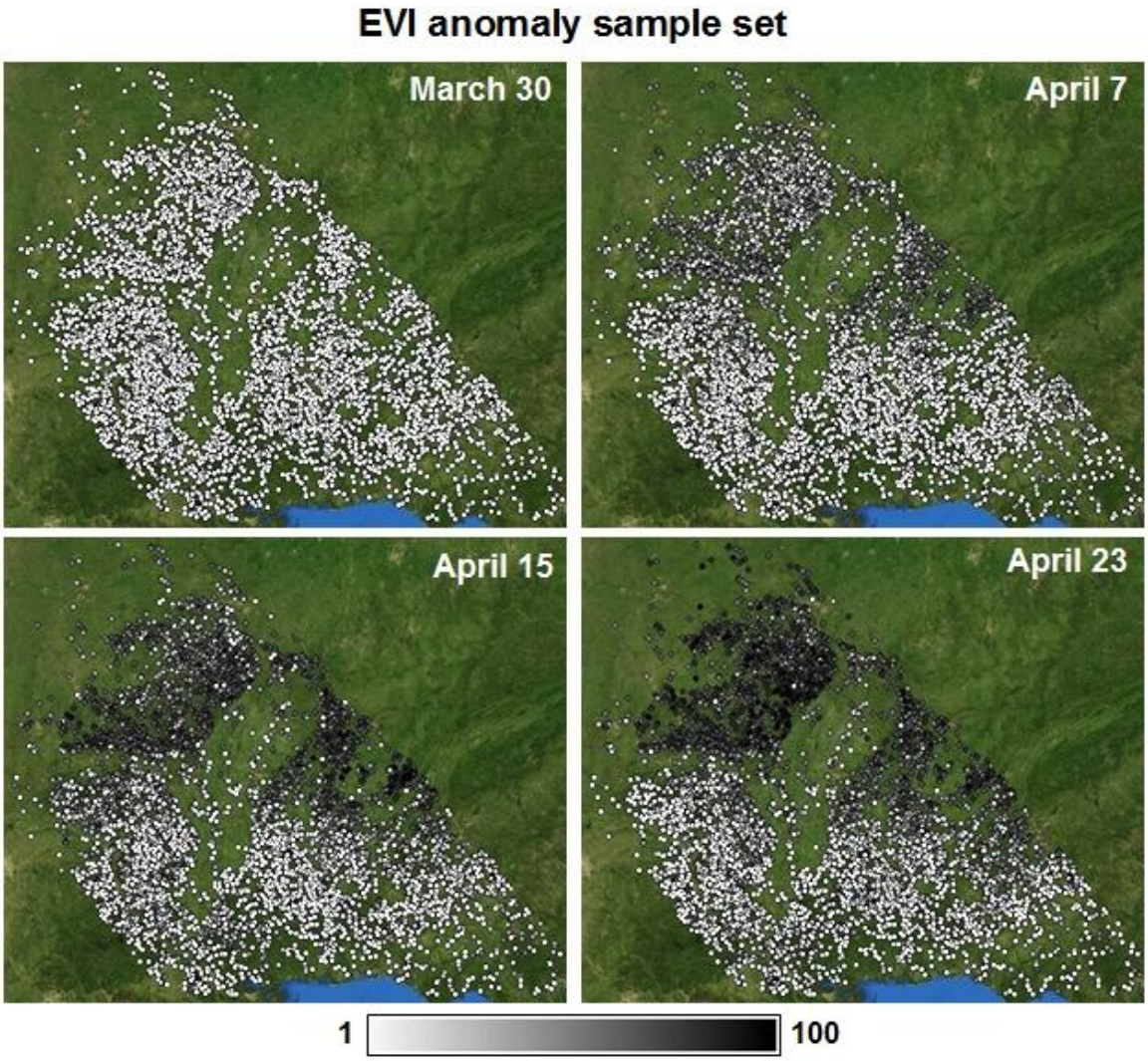

Figure 3-7 Points shaded by a grayscale color ramp represent anomalously-low EVI values of 5,000 sample sites during the four-panel, 32-day time period shown. White represents EVI values equal to or greater than the daily normal value for that location, whereas black represents the minimum value from the entire 30-day set. The darker the point, the lower the EVI value, relative to normal.

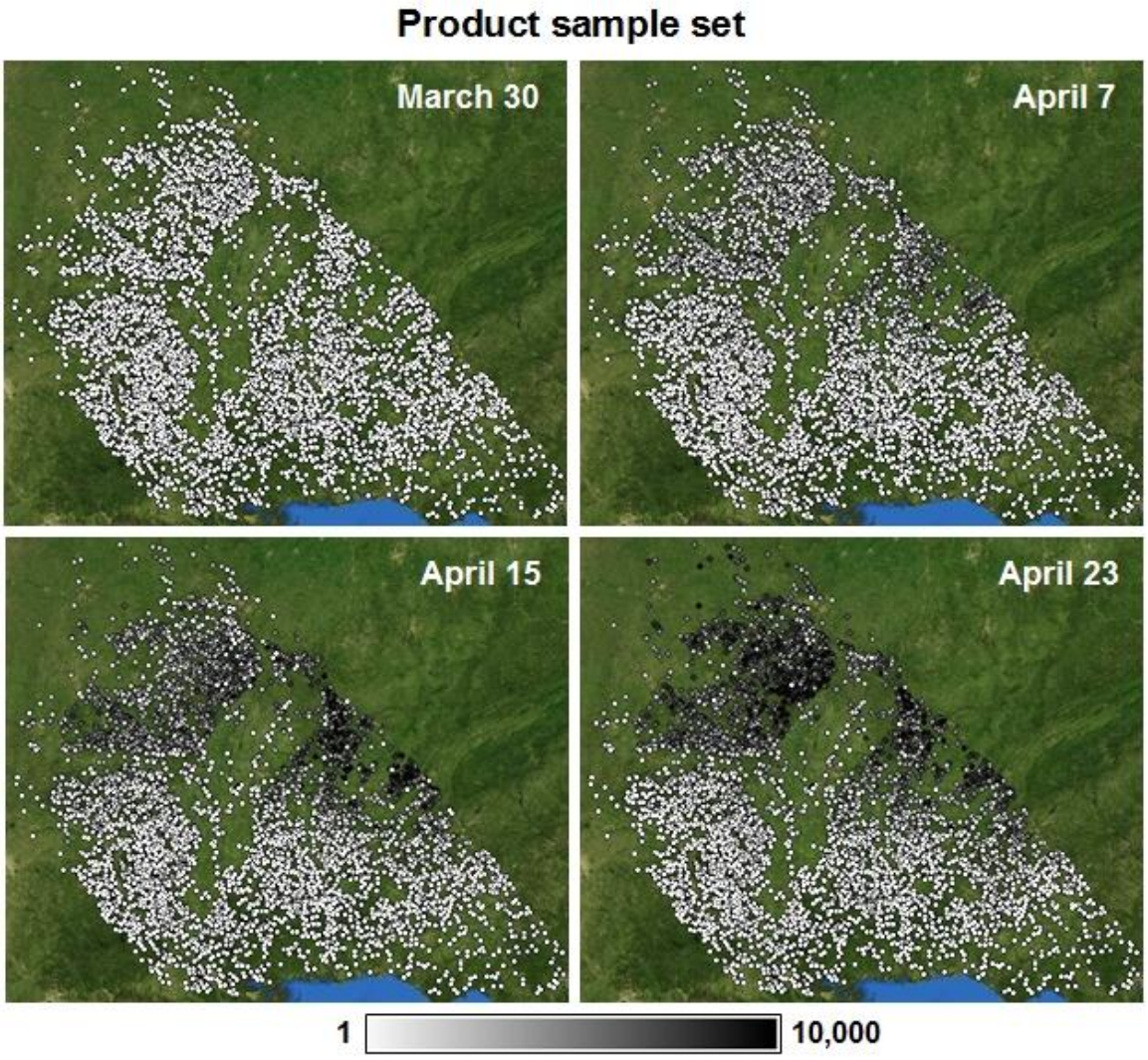

Figure 3-8 Points shaded by a grayscale color ramp represent product values (EVI anomaly × April 5-10, 2007 TMIN anomaly) of 5,000 sample sites during the four-panel, 32-day time period shown. Here, the darker the point, the higher the correlation between TMIN anomaly values (*Figure 3-3*) and EVI anomaly values (*Figure 3-7)*.

E. Calculation of spatial autocorrelation (Moran's I)

Spatial autocorrelation can be defined as the tendency for points in a dataset to cluster throughout geographic space. The spatial autocorrelation of any given dataset can be summarized using a statistic known as Moran's I. The statistic is calculated using an algorithm

that considers the specific coordinate location of every individual point in the dataset, the points' associated attribute values, and the distances between them. The coefficient returned, *I*, occupies a numerical range of -1 to +1; negative coefficients indicate a tendency for dispersion of like values, positive coefficients indicate a tendency for clustering of like values, and a coefficient of zero indicates a perfectly random distribution, as if by chance.

The rationale behind using Moran's I for quantifying the spatial congruence between the freeze map and maps of anomalously-low EVI is as follows:

If a grid featuring a particular pattern is multiplied by another grid featuring the exact same pattern in the exact same location, then the clustering of that pattern will be exaggerated in the output product grid, and as a result, Moran's I for the product will be greater than that of the input. However, if the two input grids feature patterns that are equally clustered but occupy entirely different locations (or occupy the same location but cluster differently), then multiplying them together would produce an output grid that was less clustered and more dispersed than either input, and this would be reflected by its relatively-lower Moran's I.

The hypothesis of this study is that the pattern of the freeze map is spatially congruous with the pattern of anomalously-low EVI observed after the freeze. So, if we can determine *I* for the freeze map, *I* for each of the 30 EVI anomaly rasters, and *I* for each of the 30 product rasters, then logically it should follow that post-freeze product *I* would be greater than its corresponding anomaly *I*, because its pattern would be exaggerated by the spatial congruence of the input patterns. If freeze *I* happens to be less than anomaly *I*, then we would expect product *I* to be less than anomaly *I* instead. While we would not necessarily expect to see any relationship exist prior to the freeze event, we would, however, expect to see it immediately after the date of the freeze event, and persist for some time afterwards. The length of time and degree to which

product I remains greater than *anomaly I* should indicate the duration and intensity of the persisting correlation.

Moran's I gives us information that may not be apparent by merely visualizing the maps. For example, while we may be able to compare a map of anomaly values for a particular day with the same day's map of product values or the freeze map, we cannot visually interpret the exact degree of clustering in each. This is important information to know if we are attempting to determine that the clustering is greater in one map than it is in the other. Otherwise, we are merely eyeballing any perceived correlation, and are thereby prone to inaccurate judgments.

Once the anomaly and product sample sets had been created, Moran's I was calculated for each using a GIS tool. The tool featured various settings for certain parameters, including the conceptualization of spatial relationships, the distance threshold, and the distance method. Conceptualization of spatial relationships refers to how the algorithm, when evaluating an individual point in the set, weighs the values of other points around it; with conceptualization set to 'inverse,' the impact of one value on another decreases with distance, and with conceptualization set to 'fixed,' all points in the set are weighted equally. Distance threshold is the cut-off distance from the point being evaluated, past which other points in the set will not be considered, regardless of their weight. Distance method refers to how distance is calculated, whether as a straight line between two points (Euclidean), or as along axes at right angles, like city blocks (Manhattan).

For each of the 60 sample files, the tool returned the *I* coefficient and its associated Z-score to indicate the statistical significance of *I* – that is, whether or not the null hypothesis (that there is no clustering) can be rejected. Tool settings used were inverse conceptualization, a distance threshold of 100 kilometers, and Euclidean distance method. Results from the

calculation of Moran's I are listed in *Table 4-2* and summarized graphically by *Figures 4-1* and *4-2*.

Freeze map processing

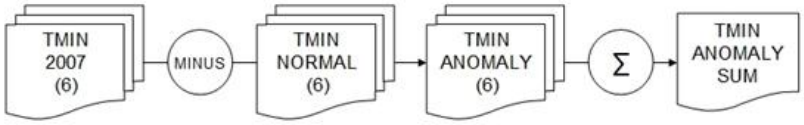

EVI anomaly map processing

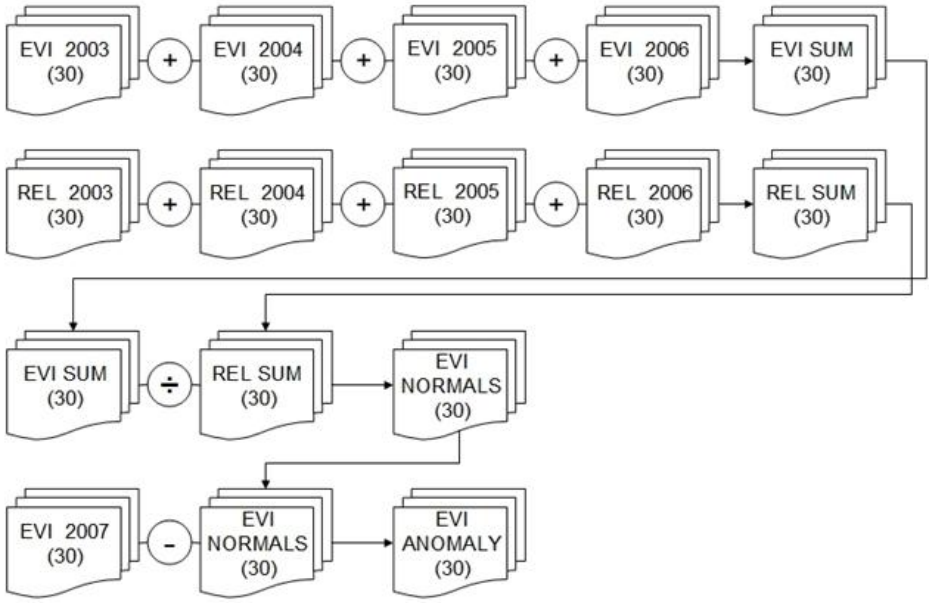

Sampling method processing

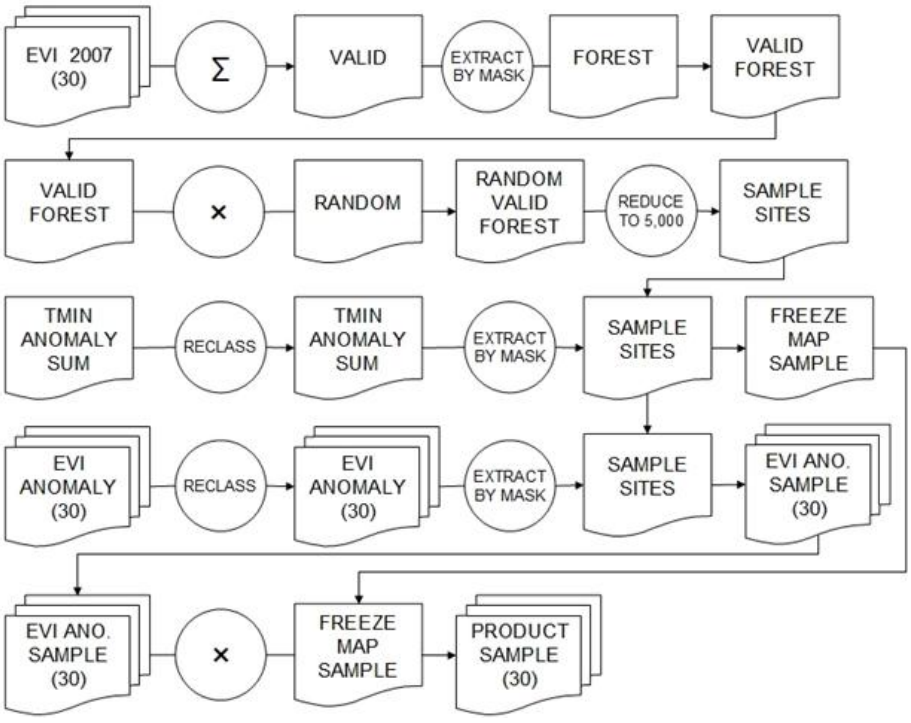

Figure 3-9 Flow chart diagram summarizing data processing steps.

IV. RESULTS AND DISCUSSION

To interpret the results, we will first consider the values of the EVI anomaly sample set over time (*Table 4-1*), and look for any changes apparent around the time of the freeze event, April 5-10. The right changes at the right time – specifically, an abrupt increase of mean values coinciding with the timing of the freeze event – will suggest a temporal correlation with the freeze event. Changes in the values of the product set relative to the timing of the freeze event could also be considered, but because its values are merely the values of the anomaly set multiplied by a constant (the freeze map), there is no additional insight to be gained through analysis of its patterns that would not otherwise be gained through analysis of the anomaly sample values themselves.

A temporal correlation between the two does suggest a causal relationship, but it does not address the spatial properties of that relationship. So, after considering the sample values, we will consider the spatial autocorrelation of those values – their tendency to cluster within space – by looking at the changes in Moran's I over time (*Table 4-2*). If indeed the pattern of the freeze map and the patterns of low forest productivity are spatially congruous with each other, then we would expect to see product *I* exceed anomaly *I* immediately following the freeze event.

By including spatial autocorrelation in the analysis, the addition of a spatial component allows us to go beyond making a determination of a merely temporal correlation and determine that a spatio-temporal correlation also exists. This additional dimension of evidence makes a determination of spatio-temporal correlation between anomalously-low EVI and anomalously-low TMIN more conclusive than a mere temporal one.

Table 4-1 Minimum, maximum, and mean values of the EVI anomaly sample set and product (EVI anomaly × TMIN anomaly) sample set.

Values of EVI anomaly sample set and product sample set							
Calendar Day	Julian Day	EVI anomaly			Product		
		Min	Max	Mean	Min	Max	Mean
Mar 8	65	1	46	4	19	2925	211
Mar 16	73	1	61	4	19	3362	288
Mar 22	81	1	54	2	19	2491	131
Mar 30	89	1	51	2	19	3276	130
Apr 7	97	1	64	10	19	6272	702
Apr 15	105	1	98	20	19	9310	1457
Apr 23	113	1	95	24	25	9310	1766
May 1	121	1	96	12	25	8352	820
May 9	129	1	90	13	25	7387	880
May 17	137	1	99	15	19	7920	1032
May 25	145	1	93	11	27	7553	741
Jun 2	153	1	97	12	27	7304	746
Jun 10	161	1	92	11	19	7553	697
Jun 18	169	1	98	13	19	8036	795
Jun 26	177	1	100	11	27	7840	661
Jul 4	185	1	100	13	25	9207	833
Jul 12	193	1	95	12	19	6650	748
Jul 20	201	1	95	12	19	7392	701
Jul 28	209	1	75	14	19	5964	908
Aug 5	217	1	84	10	19	6720	618
Aug 13	225	1	74	9	27	5487	563
Aug 21	233	1	96	10	19	8281	628
Aug 29	241	1	92	10	27	5782	647
Sep 6	249	1	68	9	25	6392	581
Sep 14	257	1	70	6	25	5740	365
Sep 22	265	1	78	6	19	4275	347
Sep 30	273	1	48	7	27	2960	387
Oct 8	281	1	40	3	25	2856	197
Oct 16	289	1	48	4	25	4608	240
Oct 24	297	1	37	3	19	2560	165

Table 4-2 Moran's I and associated Z-score for the EVI anomaly sample set and product (EVI anomaly × TMIN anomaly) sample set, evaluated using inverse distance conceptualization at a distance threshold of 100 km. Higher *I* indicates a greater tendency for clustering.

Spatial Autocorrelation (Moran's I)					
Calendar Day	Julian Day	***I* (EVI anomaly)**	*Z* (EVI anomaly)	***I* (Product)**	*Z* (Product)
Mar 8	65	**0.163317**	60.92	**0.155005**	57.80
Mar 16	73	**0.113639**	42.41	**0.223441**	83.28
Mar 22	81	**0.256319**	95.71	**0.246317**	91.93
Mar 30	89	**0.042406**	15.90	**0.089275**	33.41
Apr 7	97	**0.464913**	173.12	**0.539200**	200.75
Apr 15	105	**0.567301**	211.20	**0.662755**	246.70
Apr 23	113	**0.713381**	265.55	**0.800064**	297.76
May 1	121	**0.258470**	96.29	**0.362998**	135.19
May 9	129	**0.310015**	115.46	**0.404491**	150.60
May 17	137	**0.359597**	133.91	**0.528607**	196.80
May 25	145	**0.149268**	55.64	**0.235599**	87.78
Jun 2	153	**0.215558**	80.32	**0.274794**	102.36
Jun 10	161	**0.124629**	46.47	**0.179369**	66.85
Jun 18	169	**0.125788**	46.90	**0.182676**	68.08
Jun 26	177	**0.094764**	35.36	**0.076438**	28.54
Jul 4	185	**0.090394**	33.72	**0.129049**	48.12
Jul 12	193	**0.155134**	57.82	**0.120409**	44.89
Jul 20	201	**0.076012**	28.37	**0.099487**	37.11
Jul 28	209	**0.286642**	106.75	**0.367527**	136.85
Aug 5	217	**0.136908**	51.04	**0.233627**	87.04
Aug 13	225	**0.136326**	50.82	**0.223011**	83.09
Aug 21	233	**0.074016**	27.63	**0.129500**	48.30
Aug 29	241	**0.201721**	75.17	**0.317435**	118.23
Sep 6	249	**0.169965**	63.33	**0.191797**	71.47
Sep 14	257	**0.138543**	51.67	**0.132033**	49.26
Sep 22	265	**0.213489**	79.59	**0.155096**	57.83
Sep 30	273	**0.212714**	79.25	**0.165025**	61.49
Oct 8	281	**0.134373**	50.12	**0.083107**	31.04
Oct 16	289	**0.162635**	60.64	**0.086839**	32.44
Oct 24	297	**0.094947**	35.45	**0.073085**	27.31

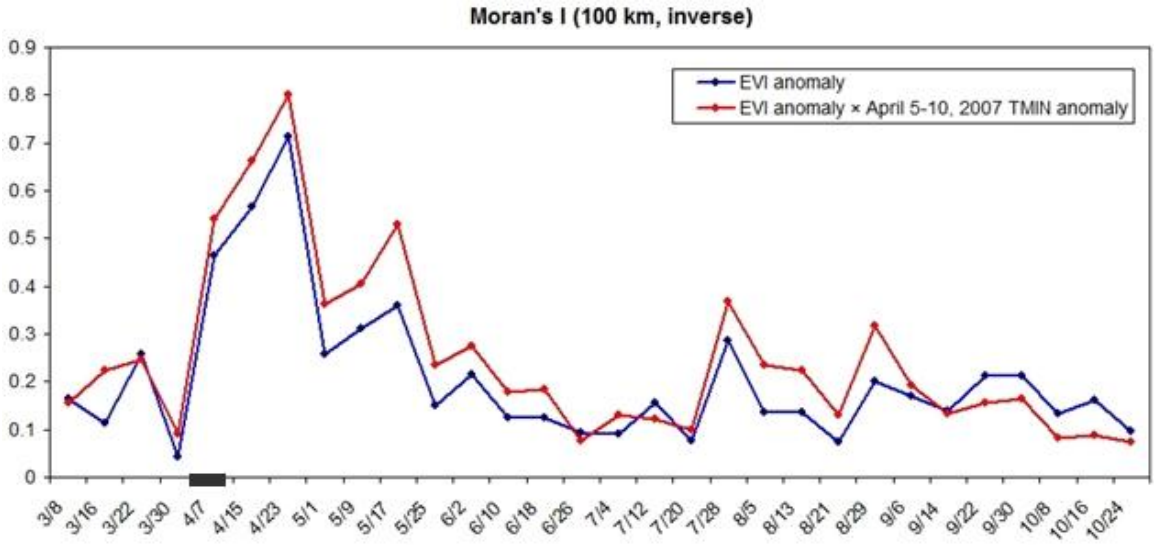

Figure 4-1 Line graph of data from *Table 4-2* depicting variation of spatial autocorrelation values (Moran's *I*) of the EVI anomaly and product datasets over time. The grey bar on the horizontal axis represents the April 5-10, 2007 freeze event.

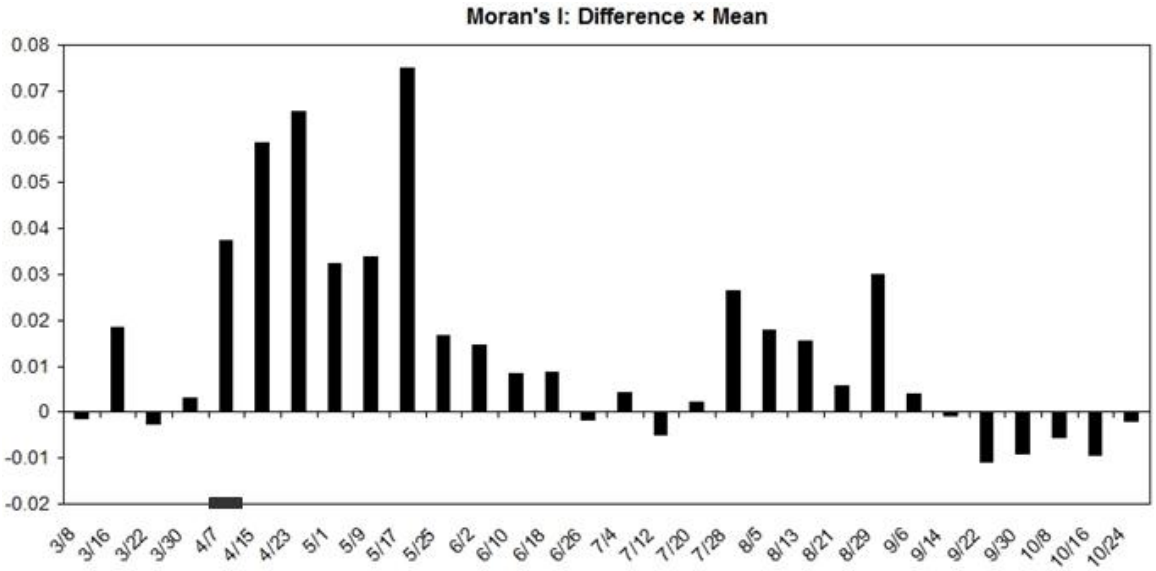

Figure 4-2 Bar graph highlighting the differences in Moran's I between the anomaly and product sets listed in *Table 4-2*. In this graph, values of *I* difference (product *I* - anomaly *I*), are multiplied by a factor of their mean [(product I + anomaly I) ÷ 2].

A. Analysis of Sample Set Values

Looking at the mean EVI anomaly values (*Table 4-1*), we can see that the lowest mean value of the entire set was featured in the imagery from March 22 (a 16-day composite of observations made from March 22-April 6) and March 30 (likewise, for March 30-April 14). The mean value, representing the most commonly-observed value in both of these images, was 2 on a scale of 1-100. This indicates a very small degree of anomalously-low EVI values during the two weeks that preceded the freeze event. It is no surprise to find a lack of unusually-low EVI values in the imagery corresponding with this two-week period, since we know that record-setting warmth was occurring regionally at the time. The March warmth is what triggered the greater-than-usual vegetative productivity, and this is reflected in the predominance of unusually-high EVI depicted in the anomaly maps for this period.

Whereas the lowest mean EVI anomaly values were observed primarily before the freeze, the highest global mean values are found in images corresponding with the freeze event and the month that followed. Mean values of 10, 20, and the global high of 24 were observed in the imagery on April 7, April 15, and April 23, respectively. After peaking in the April 23 imagery, mean values fell to the mid-to-low teen range, where they remained throughout the spring and summer before gradually tapering off in August. The spike in mean values observed after the freeze (indicating an abundance of unusually low EVI) means that forest productivity suffered its greatest losses during this period. However, this only tells us that productivity was diminished – not *where* it was diminished. To analyze the spatial aspect, we look at Moran's I scores.

B. Analysis of Spatial Autocorrelation

Taken on their own, measures of spatial autocorrelation of the EVI anomaly sample set do not provide any insight into a potential spatial relationship with the freeze map. Meaningful interpretation of the Moran's I scores requires using anomaly set *I* as a baseline by which to evaluate product set *I*. Once again, this is because we are interested in knowing whether or not the clustering of a particular day's EVI anomaly map multiplied by the freeze map is greater than the clustering of that day's EVI anomaly map alone, and *I* summarizes that clustering.

Table 4-1 lists the Moran's I scores returned for the EVI anomaly set and the product set, and *Figure 4-1* provides a graphical summary of these scores. When both scores show clustering at a significant level, then the difference between product *I* and anomaly *I* can be thought of as being directly proportional to the degree of spatial correlation between the freeze (low TMIN anomaly) and freeze damage (low EVI anomaly). The more positive the difference, the more similar their patterns are; the more negative the difference, the more dissimilar they are. The values in *Figure 4-2* highlight *I* difference by multiplying it by a factor of the two scores' mean value. The resulting index is more useful for analyzing trends in spatial congruence over time than merely *I* difference, because the significance of any particular *I* difference is greater when clustering is significant to begin with.

Prior to the date of the freeze, *I* for both datasets is low, although *I* difference varies considerably. This makes sense, since patterns of pre-freeze EVI anomaly could obviously not possess any congruence with patterns of a freeze that had not yet occurred. Thus, any correlation at this point in time could only be the result of random chance, and since clustering does not occur at a significant level anyway, the difference is essentially negligible.

As soon as the freeze occurs, an abrupt change in *I* difference dynamics becomes apparent, beginning with the April 7 dataset. Clustering levels from the first three images during the period of peak response (April 7-23) are the greatest levels of clustering observed throughout the entire set. For 10 consecutive weeks after the freeze, Product *I* is greater than anomaly *I*, though the difference becomes less apparent during the last few weeks of this trend. On June 26, a month-long period of persistently low clustering occurs. This is likely the result of large portions of "marginal"-quality pixel data appearing in these images due to atmospheric contamination brought on by persistent summer thunderstorm activity occurring throughout the region at this time. The EVI anomaly maps for this period show large gaps where unreliable pixels had been removed, and this likely affected the quality of pixel data surrounding those gaps, which in turn impacted measures of spatial autocorrelation.

Clustering increases again somewhat during August, but values remain relatively low and do not approach the greatest levels observed during the peak response period of April and May. During the last five weeks of observations through mid-September and October, anomaly I was consistently greater than product I, although by this time any clustering had subsided enough to the point where it was essentially insignificant.

C. Rejection of Null Hypothesis

After analyzing spatial autocorrelation values of the anomaly sample set and product sample set, we find that the greatest spatial correlation between anomalously-low TMIN and anomalously-low EVI occurs over April and May, 2007. This spatial correlation between the pattern of the freeze and the freeze response seems to corroborate the temporal correlation evident from analysis of the sample set values that show a sudden increase in unusually-low EVI

as soon as the freeze occurs. Therefore, we can reject the null hypothesis that patterns of unusually-low forest productivity following an April 2007 freeze event are not spatially congruous with the pattern of unusually-low temperatures sustained during the freeze event. In rejecting the null hypothesis, we accept the alternative hypothesis that the freeze and subsequent low productivity are indeed spatially congruous.

V. CONCLUSION AND FUTURE WORK

Deciduous forests throughout the U.S. interior were indeed impacted by the spring 2007 freeze in a meaningful and lasting way. Of the land represented by the imagery used, the region that most prominently exhibited a freeze response was the Ozark mountain region of northern Arkansas and southern Missouri. Areas featuring the least freeze response included the Mississippi delta and the plains regions of west Kansas and southern Oklahoma. Impacts were most prominent during the first 10 weeks after the freeze. The results of this study are consistent with those of Gu (2008), who identified the productivity response as occurring at the same time (peaking in late April, continuing through May) and at the same place (a retreat of the vernal front from northern Missouri to the deep South) as this study.

This study has been successful in demonstrating a geographically-based method of identifying patterns common among two independently-obtained sets of spatial data, despite those datasets measuring two distinctly different environmental variables, with two distinctly different means of acquisition. It is clear from review of the EVI anomaly maps and from the confirmation of spatial correlation performed by this study, that regional patterns of decreased productivity among deciduous forests can and will follow significant spring freeze events, often prolonged for months afterwards.

Future enhancements to the study might include the inclusion of additional tiles of imagery, since freeze impacts throughout Tennessee and the Carolinas were reported, but are not represented by the MODIS tile used. Increased temporal resolution of the freeze map via usage of hourly TMIN data, as opposed to daily, would potentially promote a more accurate model of freeze severity, although data at this scale is difficult to acquire. Furthermore, the inclusion of other environmental factors known to contribute to freeze damage – most notably any

unseasonable warmth that may have preceded it, but also wind speed, humidity, and elevation – might increase the robustness of the model.

An example of a potential practical application for this study is environmental forecasting. The incorporation of satellite imagery and terrestrial weather observations into real-time global environmental forecasts is currently being practiced by NASA's Terrestrial Observation and Prediction System (TOPS). The spatio-temporal relationship between temperatures and productivity analyzed by this study could be applied to the development of a predictive model similar to the satellite-based terrestrial carbon flux model TOPS is currently developing (Nemani, 2005). For instance, one such model could forecast large-scale reductions in forest productivity based on the meteorological properties of cold fronts that surpass a certain threshold indicative of potential damage, and occur during the phenological stages most vulnerable to spring freeze damage.

In the same way, this model could be beneficial to relatively longer-term forecasts of climate. Other studies have shown that unusually warm early spring seasons contribute as much, if not more, to freeze damage following premature onset of growth (Gu, 2008). Given that global average temperatures are known to be rising (Menzel and Fabian, 1999) without a corresponding decrease in the frequency of spring freeze events (Cannell, 1986; Mulholland 1999; Linkosalo, 2000), a logical inference is that decreased rates of forest productivity can be expected in the future. Forests provide a vital terrestrial carbon sink because of their capacity for large-scale respiration, so decreased forest productivity has the potential to inhibit rates of carbon fixation, and exacerbate global climate change by doing so. This is one of many positive feedback loop mechanisms that drive climate change, and since climate scientists are constantly

searching for ways to improve their models, the incorporation of such a feedback mechanism into their models would be of value to the scientific community at large.

VI. LIST OF REFERENCES

Ahl, D.E., S.T. Gower, S.N. Burrows, N.V. Shabanov, R.B. Myeni, and Y. Knyazikhin, 2006, "Monitoring Spring Canopy Phenology of a Deciduous Broadleaf Forest using MODIS," *Remote Sensing of Environment*, 104:88-95.

Beerling, D.J., A.C. Terry, P.L. Mitchell, T.V. Callaghan, D. Gywnn-Jones, and J.A. Lee, 2001, "Time to Chill: Effects of Simulated Global Change on Leaf Ice Nucleation Temperatures of Subarctic Vegetation," *American Journal of Botany*, 88:628-633.

Cannell, M.G.R. and Smith, R.I., 1986, "Climatic Warming, Spring Budburst and Frost Damage on Trees," *Journal of Applied Ecology*, 23:177-191.

Chen, X., L. Vierling, D. Deering, and A. Conley, 2005, "Monitoring Boreal Forest Leaf Area Index across a Siberian Burn Chronosequence: a MODIS Validation Study," *International Journal of Remote Sensing*, 26(24):5433-5451.

Dawson, T.P., P.R.J. North, S.E. Plummer, and P.J. Currian, 2003, "Forest Ecosystem Chlorophyll Content: Implications for Remotely Sensed Estimates for Net Primary Productivity," *International Journal of Remote Sensing*, 24(3):611-617.

Dittmar, C., W. Fricke, W. Elling, 2006, "Impact of Late Frost Events on Radial Growth of Common Beech in Southern Germany," *European Journal of Forest Research*, 125:249-259.

Fisher, J.I., J.F. Mustard, M.A. Vadeboncoeur, 2005, "Green Leaf Phenology at Landsat Resolution: Scaling From the Field to the Satellite," *Remote Sensing of Environment*, 100:265-279.

Gorsuch, D.M. and Oberbauer, S.F., 2002, "Effects of Mid-Season Frost and Elevated Growing Season Temperature on Stomatal Conductance and Specific Xylem Conductivity of the Arctic Shrub, *Salix Pulchra*," *Tree Physiology*, 22:1027-1034.

Gu, L., T. Meyers, S.G. Pallardy, P.J. Hanson, B. Yang, M. Heuer, K.P. Hosman, J.S. Riggs, D. Sluss, S.D. Wullschleger, 2006, "Direct and Indirect Effects of Atmospheric Conditions and Soil Moisture on Surface Energy Partitioning Revealed by a Prolonged Drought at a Temperate

Forest Site," *Journal of Geophysical Research-Atmosphere*, D16102, doi:10.1029/2006JD007161.

Gu, L., P.J. Hanson, W.M. Post, D.P. Kaiser, B. Yang, R. Nemani, S.G. Pallardy, and T. Meyers, 2008, "The 2007 Eastern US Spring Freeze: Increased Cold Damage in a Warming World?," *BioScience*, 58(3):253-262.

Hanninen, H., 1991, "Does Climatic Warming Increase the Risk of Frost Damage in Northern Trees?," *Plant, Cell, and Environment*, 14:449-454.

Hanninen, H., 2006, "Climate Warming and the Risk of Frost Damage to Boreal Forest Trees: Identification of Critical Ecophysiological Traits," *Tree Physiology*, 26:889-898.

Haworth, R. and Spiers, A., 1992, "Isolation of *Xanthomonas campestris* PV *populi* from stem lesions on *Salix matsudana X alba* Aokautere in New Zealand," *European Journal of Plant Pathology*, 22:247-251.

Houborg, R., H. Soegaard, and E. Boegh, 2007, "Combining Vegetation Index and Model Inversion Methods for the Extraction of Key Vegetation Biophysical Parameters Using Terra and Aqua MODIS Reflectance Data," *Remote Sensing of Environment*, 106(1):39-58.

Huete, A.R., Didan, K., Miura, T., Rodriguez, E.P., Gao, X. and G. Ferreira, 2002, "Overview of the Radiometric and Biophysical Performance of the MODIS Vegetation Indices," *Remote Sensing of Environment*, 83:195-213.

Inouye, David W., 2000, "The Ecological and Evolutionary Significance of Frost in the Context of Climate Change," *Ecology Letters*, 3:457-463.

Jenkins, J.P., Braswell, B.H., Frolking, S.E., *et al*., 2002, "Detecting and Predicting Spatial and Interannual Patterns of Temperate Forest Springtime Phenology in the Eastern U.S.," *Geophysical Research Letters*, 29(24):54.1-54.4

Jensen, John R. *Introductory Digital Image Processing: A Remote Sensing Perspective*. Upper Saddle River, NJ: Prentice-Hall, 2005.

Kellomaki, S., H. Hanninen, and M. Kolstrom, 1995, "Computations on Frost Damage to Scots Pine Under Climatic Warming in Boreal Conditions," *Ecological Applications*, 5(1):42-52.

Kramer, K., A. Friend, and I. Leinonen, 1996, "Modeling Comparison to Evaluate the Importance of Phenology and Spring Frost Damage for the Effects of Climate Change on Growth of Mixed Temperate-Zone Deciduous Forests," *Climate Research*, 7:31-41.

Kramer, K., I. Leinonen, and D. Loustau, 2000, "The Importance of Phenology for the Evaluation of Impact of Climate Change on Growth of Boreal, Temperate, and Mediterranean Forest Ecosystems: An Overview," *International Journal of Biometeorology*, 44:67-75.

Kratsch, H.A. and Wise, R.R., 2000, "Invited Review: The Ultrastructure of Chilling Stress," *Plant, Cell and Environment*, 23:337-350.

Lederer, W. and Seemuller, E., 1992, "Investigations on the Predisposition of Strawberry Plants to Crown Rot (*Phytophthora cactorum*)," *Journal of Plant Diseases and Protection*, 99:225-233.

Linkosalo, T., T.R. Carter, R. Hakkinen, and P. Hari, 2000, "Predicting Spring Phenology and Frost Damage Risk of *Betula* spp. Under Climatic Warming: A Comparison of Two Models," *Tree Physiology*, 20:1175-1182.

Loveys, B.R., J.J.G. Egerton, M.C. Ball, 2006, "Higher Daytime Leaf Temperatures Contribute to Lower Freeze Tolerance under Elevated CO_2," *Plant, Cell, and Environment*, 29:1077-1086.

Lutze, J.L., J.S. Roden, C.J. Holly, J. Wolfe, J.J.G. Egerton, and M.C. Ball, 1998, "Elevated Atmospheric CO_2 Promotes Frost Damage in Evergreen Tree Seedlings," *Plant, Cell, and Environment*, 21:631-635.

Menzel, A. and Fabian, P., 1999, "Growing Season Extended in Europe." *Nature*, 397, 659.

Mulholland, P.J., Roberts, B.J., Hill, W.R., and Smith, J.G., 2009, "Stream Ecosystem Reponses to the 2007 Spring Freeze in the Southeastern United States: Unexpected Effects of Climate Change," *Global Change Biology*, 15:1767-1776.

Nemani, R., *et al.*, 2005, "Terrestrial Observation and Prediction System (TOPS): Developing Ecological Nowcasts and Forecasts by Integrating Surface, Satellite and Climate Data with

Simulation Models," Research and Economic Applications of Remote Sensing Data Products. American Geophysical Union.
NOAA (2007, May 9). "April 2007 Cold Wave." National Oceanic and Atmospheric Administration. Retrieved March 2010, from http://www.ncdc.noaa.gov/special-reports/2007-apr-cold-event.html

NOAA (2010, July 31). "CLIMATE SUMMARY FROM DECEMBER 2006 THROUGH MARCH 2007." National Oceanic and Atmospheric Administration, Climate Prediction Center. Retrieved September 2010, from http://www.erh.noaa.gov/rnk/Newsletter/Spring_2007/winter06_07_summary/WINTER07_article.htm

Oksanen, E., V. Freiwald, N. Prozherina, M. Rousi, 2005, "Photosynthesis of Birch (*Betula Pendula*) is Sensitive to Springtime Frost and Ozone," *Canadian Journal of Forest Research*, 35:703-712.

Olofsson, P., L. Eklundh, F. Lagergren, P. Jönsson, and A. Lindroth, 2007, "Estimating Net Primary Production for Scandinavian Forests using Data from Terra/MODIS," *Advances in Space Research,* 39:125-130.

ORNL Review (2007). "The 2007 Easter Freeze – ORNL Review Vol. 40, No. 3, 2007" Oak Ridge National Laboratory. Retrieved September 2010, from http://www.ornl.gov/info/ornlreview/v40_3_07/article08.shtml

Paige, K.N., 1992, "The Effects of Fire on Scarlet Gilia—An Alternative Selection Pressure to Herbivory," *Oecologia*, 92:229-235.

Paul, N., 1993, "Mycoherbicides and Other Biocontrol Agents for *Senecio* spp.," *Pesticide Science,* 37:323-329.

Raulier, F. and Bernier, P.Y., 2000, "Predicting the Date of Leaf Emergence for Sugar Maple Across its Native Range," *Canadian Journal of Forest Research,* 30:1429-1435.

Richardson, A.D., Bailey, A.S., Denny, E.G., Martin, C.W., and O'Keefe, J., 2006, "Phenology of a Northern Hardwood Forest Canopy," *Global Change Biology,* 12:1174-1188.

Schwartz, M.D. and Reed, B.C., 1999, "Surface Phenology and Satellite Sensor-Derived Onset of Greenness: An Initial Comparison," *International Journal of Remote Sensing*, 20(17):3451-3457.

Schwartz, M.D., Reed, B.C., White, M.A., 2002, "Assessing Satellite-Derived Start-of-Season Measures in the Coterminous USA," *International Journal of Climatology*, 22:1793-1805.

Sperry, J.S. and Sullivan, J.E.M., 1992, "Xylem Embolism in Response to Freeze-Thaw Cycles and Water Stress in Ring-Porous, Diffuse-Porous, and Conifer Species," *Plant Physiology*, 100:605-613.

University of Tennessee (2010). "The Spring 2007 Freeze." UT AgResearch, Forest Resources Research and Education Center. Retrieved October 5, 2010, from http://forestry.tennessee.edu/springfreeze07.htm

Watson, R.T., D.L. Albritton, and T. Barker, et al., 2001, *Climate Change 2001: Synthesis Report*. IPCC, Geneva, Switzerland.

Windham, A.S., 2008. "Implications of the Spring Freeze of 2007." Proceedings of the International Plant Propagators' Society. Vol. 57: 38-39.

White, M.A., Thornton, P.E., and Running, S.W., 1997, "A Continental Phenology Model for Monitoring Vegetation Responses to Interannual Climatic Variability," *Global Biogeochemical Cycles*, 11(2):217-234.

Zasada, J.C., R.M. Teclaw, D.S. Buckley, and J.G. Isebrands. 1999. Effects of frost on hardwood regeneration in northern Wisconsin. P. 17-24 in Stringer, J.W., and D.L. Loftis (eds.). Proceedings, 12th Central Hardwood Forest Conference. USDA Forest Service Southern Research Station Gen. Tech. Rep. SRS-24.